Precambrian Research xxx (2012) xxx–xxx

Contents lists available at SciVerse ScienceDirect

Precambrian Research

journal homepage: www.elsevier.com/locate/precamres

REE geochemistry of carbonates from the Guanmenshan Formation, Liaohe Group, NE Sino-Korean Craton: Implications for seawater compositional change during the Great Oxidation Event

Hao-Shu Tang[a,b], Yan-Jing Chen[b,c,*], M. Santosh[d], Hong Zhong[a], Tao Yang[e]

[a] State Key Laboratory of Ore Deposit Geochemistry, Institute of Geochemistry, Chinese Academy of Sciences, 46 Guanshui Road, Guiyang 550002, China
[b] Key Laboratory of Crustal and Orogenic Evolution, Peking University, Beijing 100871, China
[c] Key Laboratory of Mineralogy and Metallogeny, Guangzhou Institute of Geochemistry, Chinese Academy of Sciences, Guangzhou 510640, China
[d] Division of Interdisciplinary Science, Faculty of Science, Kochi University, Kochi 780-8520, Japan
[e] State Key Laboratory for Mineral Deposits, Nanjing University, Nanjing 210093, China

ARTICLE INFO

Article history:
Received 3 July 2011
Received in revised form 29 January 2012
Accepted 10 February 2012
Available online xxx

Keywords:
Great Oxidation Event
Chemical sediment
Geochemistry
REY
Seawater composition
Liaohe Group
Sino-Korean Craton

ABSTRACT

The worldwide 2.33–2.06 Ga positive $\delta^{13}C_{carb}$ excursion has been correlated with the Great Oxidation Event (GOE) and termed as the Lomagundi Event. The 2.3−1.85 Ga Guanmenshan Formation in the Liaohe Group of the northeastern Sino-Korean Craton is characterized by positive $\delta^{13}C_{carb}$ excursion and is a potential candidate to evaluate the Lomagundi Event using REY (rare earth element and yttrium, REE + Y) chemical fingerprints. Here we present major and trace element analysis of 42 samples from the Guanmenshan Formation which are pure marine chemical sediments and use the data to trace the seawater composition during 2.3–1.85 Ga. 15 least altered dolomicrite samples (>600 m strata) have $\sum$REE values of 0.739–4.175 ppm (2.414 ± 1.184 ppm) and the Y/Ho ratios of 34.5–56.6 (44.1 ± 5.7). They show uniform positive La_{SN}/La_{SN}^* (1.04 ± 0.27) and Gd_{SN}/Gd_{SN}^* (1.64 ± 0.40) anomalies, and notable LREE depletions indicated by Nd_{SN}/Yb_{SN} values of 0.24–0.92 (average 0.56 ± 0.19). These features are consistent with the geochemistry of well-oxygenated, shallow ambient seawater, and suggest that these samples provide a robust record of the primary REY signature of seawater during the Lomagundi Event. The REY patterns of 15 silicified dolomites/marbles (locally with veinlets) from the Pb–Zn mining camps in the region, with average Eu_{CN}/Eu_{CN}^* = 1.56 ± 0.95, are identical to those of high-temperature hydrothermal fluids (>250 °C), characterized by a flat pattern and marked positive Eu anomalies, indicating that these rocks were subjected to metasomatism by hydrothermal fluids. The Guanmenshan Formation shows average Ce_{SN}/Ce_{SN}^* of 0.93 ± 0.09 and Sm_{CN}/Yb_{CN} of >1 which are higher than those of the Archean (>2.33 Ga) chemical sediments (generally <1), suggesting that the REY geochemical characteristics of the carbonates from our study area were dominantly controlled by the nature of atmosphere–hydrosphere system, such as fO_2 and pCO_2. The REY in the dolomicrite were mainly sourced from fluxes of solutes from terrestrial weathering, and also from seafloor hydrothermal processes on a subordinate scale. The Guanmenshan dolomicrites have Eu_{SN}/Eu_{SN}^* values of 1.34–2.55, i.e. around 1.53, indicating that they were deposited during 2.33–2.06 Ga, as the $Eu_{SN}/Eu_{SN}^* \approx 1.53$ can be used as a proxy for the 2.33–2.06 Ga marine chemical sediments. Our study shows that the Guanmenshan Formation was formed at a critical turning point in Earth history when the global atmosphere–hydrosphere system witnessed a dramatic change from reducing to oxidizing conditions.

1. Introduction

The Archean/Proterozoic (Ar/Pt) transition in Earth history witnessed dramatic changes which include the formation of numerous cratonic basins in the Proterozoic as against the widespread greenstone belts in the Archean. From the start of Proterozoic, voluminous red beds, evaporites, stromatolite-bearing carbonates, Superior-type banded iron formation (BIF), phosphate, magnesite and rare earth element deposits were formed (Tu et al., 1985; Chen, 1990; Chen et al., 1991; Chen and Cai, 2000; Huston and Logan, 2004; Jiang et al., 2004; Tang et al., 2009, 2011; Zhai and Santosh, 2011; Zhao, 2010; and references therein). The tectonic processes and global environmental change during the Paleoproterozoic world from 2.5 to 1.6 Ga has been the focus of numerous studies in the past. Schidlowski et al. (1975, 1976) first

* Corresponding author at: Peking University, Key Laboratory of Crustal and Orogenic Evolution, Beijing 100871, China. Tel.: +86 10 62757390.
E-mail address: yjchen@pku.edu.cn (Y.-J. Chen).

0301-9268/$ – see front matter © 2012 Elsevier B.V. All rights reserved.
doi:10.1016/j.precamres.2012.02.005

Please cite this article in press as: Tang, H.-S., et al., REE geochemistry of carbonates from the Guanmenshan Formation, Liaohe Group, NE Sino-Korean Craton: Implications for seawater compositional change during the Great Oxidation Event. Precambrian Res. (2012), doi:10.1016/j.precamres.2012.02.005

discovered the positive $\delta^{13}C_{carb}$ anomaly in the ~2.0 Ga carbonates from Karelia (Russia) and the Fennoscandian Shields, as well as in the dolomites with ages of 2.65−1.95 Ga from the Lomagundi Province (Zimbabwe). They also related this phenomenon to the oxidation of the atmosphere. However, this important discovery had been largely neglected prior to 1990.

Taylor and McLenna (1985) documented the discrepancy in element geochemistry (particularly in rare earth elements) between Archean and post-Archean shales, and related it to the change in crustal compositions resulting from extensive development of granitoids with ages of 3.0−2.5 Ga. Chen and co-authors (Chen and Fu, 1991, 1992; Chen et al., 1992, 1996; Chen and Zhao, 1997; Chen and Su, 1998) discovered that the pre- and post-2.3 Ga sediments (both chemical and clastic) from the Sino-Korean Craton show contrasting REE patterns (normalized to chondrite), and correlated this difference to a Great Oxidation Event (GOE) at ca. 2.3 Ga in terms of SHAB (soft and hard acids and bases) theoretical synthesis, and proposed that an environmental catastrophe might have occurred at ca. 2.3 Ga (Chen, 1988, 1990; Chen et al., 1991, 1994, 1996, 1998, 2000). In 1989, the International Commission on Stratigraphy recommended 2.3 Ga as the boundary between the Siderian and the Rhyacian in the Precambrian Stratigraphy chart. Thereafter, more and more geologists focused their attention to the nature of the 2.3 Ga stratigraphic boundary and recognized the worldwide positive $\delta^{13}C_{carb}$ excursions in the 2.33−2.06 Ga carbonate strata (Schidlowski, 1988; Bekker et al., 2003a,b, 2006; Tang et al., 2004, 2011; and references therein). The positive $\delta^{13}C_{carb}$ excursion was variously termed as the Lomagundi Event (Karhu and Holland, 1996), the Jatulian Event (Melezhik and Fallick, 1996; Melezhik et al., 1999) or the Great Oxidation Event (Anbar et al., 2007; Konhauser et al., 2009; Zhao, 2010) and was genetically correlated to global environmental changes (Karhu and Holland, 1996; Melezhik et al., 1999; Chen et al., 2000), or to the breakup of the Kenorland/Superia supercontinent (Bekker and Eriksson, 2003).

The recognition of the GOE or environmental catastrophe was one of the most important progresses in the research on the Precambrian, and provided insights into our understanding of the Precambrian evolution and mineralization during the early Earth history. The stratochemical studies of the event mainly relied on carbon and oxygen isotopes, and partly on sulfur isotopes (Karhu and Holland, 1996; Buick et al., 1998; Bekker et al., 2001, 2003a,b, 2006; Melezhik et al., 1997, 1999; Melezhik and Fallick, 1996; Tang et al., 2011). The composition of the marine chemical sediments is comprehensively controlled by various environmental factors. Trace element and isotope inventories of the marine chemical sediments, such as BIFs, reflect both the input of mantle-sourced and terrestrial components and earth's surficial environment changes, including the compositional evolution of seawater through geologic time (Huston and Logan, 2004; Frei et al., 2008).

The usefulness of rare earth elements and yttrium (REY) as seawater proxies has been studied by many scientists (e.g., Bau and Dulski, 1996; Webb and Kamber, 2000; Shields and Stille, 2001; Kamber and Webb, 2001; Nothdurft et al., 2004; Shields and Webb, 2004; Bolhar et al., 2004; Bolhar and Van Kranendonk, 2007; Frei et al., 2008; Alexander et al., 2008). The REY signatures can provide information on secular changes in input source flux and oxygenation (e.g., Chen and Zhao, 1997; Kamber and Webb, 2001; Nothdurft et al., 2004; Alexander et al., 2008), thereby providing insights on the characters and secular changes in the composition of the continental crust, tectonic setting and surficial environment (Chen, 1996; Nothdurft et al., 2004). Information concerning water depth, oceanic circulation and stratification, paleogeography and depositional models have also been derived from such studies (Bau and Dulski, 1996; Kamber and Webb, 2001; Alexander et al., 2008).

The Sino-Korean Craton (Fig. 1) preserves widespread Paleoproterozoic strata, such as those of the Liaohe Group in the eastern Liaoning Province. However, it is unclear whether these strata record the GOE or Lomagundi Event. We have recently reported the discovery of Paleoproterozoic positive $\delta^{13}C_{carb}$ excursion in the Guanmenshan Formation of the Liaohe Group, northeastern Sino-Korean Craton (Tang et al., 2011). In this contribution we attempt to use the REY fingerprint to study the 2.3−1.85 Ga carbonate strata from the Guanmenshan Formation, and evaluate the related issues on the Lomagundi Event or GOE in the Sino-Korean Craton.

2. Geology and stratigraphy

Recent models propose that the Precambrian crustal evolution history of the Sino-Korean Craton involved three main phases: (1) a major phase of continental growth at ca. 2.7 Ga; (2) the amalgamation of micro-blocks and cratonization at ca. 2.5 Ga; and (3) Paleoproterozoic rifting–subduction–accretion–collision tectonics and subsequent high-grade granulite facies metamorphism–granitoid magmatism during ca. 2.0–1.82 (Zhai and Santosh, 2011; and references therein; Wan et al., 2011). The Precambrian basement of the Sino-Korean Craton can be divided into the Eastern and Western Blocks dissected by three major Paleoproterozoic accretionary belts, namely, the Khondalite Belt or the Inner Mongolia Suture Zone, the Trans-North China Orogen or the Central Orogenic Belt and the Jiao-Liao-Ji Belt (Fig. 1; Zhao et al., 2005; Santosh, 2010; Liu et al., 2011; Zhai and Santosh, 2011; Kusky, 2011; Santosh et al., 2011). The roughly EW-trending Khondalite Belt or the Inner Mongolia Suture Zone is interpreted as a Paleoproterozoic collisional belt along which the Yinshan and Ordos Blocks amalgamated to form the Western Block (Zhao et al., 2005; Santosh et al., 2006, 2007a,b, 2008, 2009, 2011; Wan et al., 2006; Xia et al., 2006a,b; Yin et al., 2009; Santosh, 2010; Tsunogae et al., 2011), which then collided with the Eastern Block along the Trans-North China Orogen to form the basement of the Sino-Korean Craton (Fig. 1; Guo et al., 2002, 2005; Kröner et al., 2005, 2006; Zhao et al., 2005, 2006; Liu et al., 2006; Zhang et al., 2006, 2007, 2009; Kusky, 2011; Zhai and Santosh, 2011).

The northeast part of the Sino-Korean Craton includes the Liaobei, Longgang and Helong terrains in the north, the Liaonan and Langlin terrains in the south, and the Jiao-Liao-Ji Belt in the middle (Fig. 2). These terrains (or belts) comprise Archean granite–greenstone associations and Paleoproterozoic lithostratigraphic successions (Jiang, 1984; Zhang et al., 1988; Sun et al., 1993, 1996; Jiang et al., 1997, 2004; Li et al., 2004, 2005, 2006; Zhao et al., 2004, 2005; Wan et al., 2006; Li and Zhao, 2007; Tam et al., 2011; Zhai and Santosh, 2011). The Jiao-Liao-Ji Belt, however, is mainly composed of Paleoproterozoic sedimentary and volcanic successions that are metamorphosed in the greenschist to lower amphibolite facies and tectonically associated with granitic and mafic intrusions (Li et al., 2004, 2005, 2006). Terrains in the northern or southern domains of the Jiao-Liao-Ji belt mainly consist of Archean granite–greenstone associations and locally developed Paleoproterozoic strata. All of the Paleoproterozoic successions are comparable with respect to lithology and ages, but are variably called the Macheonayeong Group in North Korea, the Ji'an and Laoling Groups in southern Jilin, the Liaohe Groups in the eastern Liaoning Peninsula (Zhao et al., 2005) and the northern Liaohe Group in the Liaobei terrain (Wang et al., 1989), or are simply termed the Liaohe Group (Tang et al., 2004). In this paper, we use the term Liaohe Group and focus on the Paleoproterozoic strata of the Liaobei terrain.

The Paleo–Mesoproterozoic sedimentary assemblage in the Liaobei terrain was deposited mainly in the Fanhe Basin (Fig. 3) and is composed of weakly metamorphosed intermediate-felsic volcanic rocks, feldspathic quartzarenite and carbonates that unconformably overlie the Archean Anshan Group (Liaoning

Please cite this article in press as: Tang, H.-S., et al., REE geochemistry of carbonates from the Guanmenshan Formation, Liaohe Group, NE Sino-Korean Craton: Implications for seawater compositional change during the Great Oxidation Event. Precambrian Res. (2012), doi:10.1016/j.precamres.2012.02.005

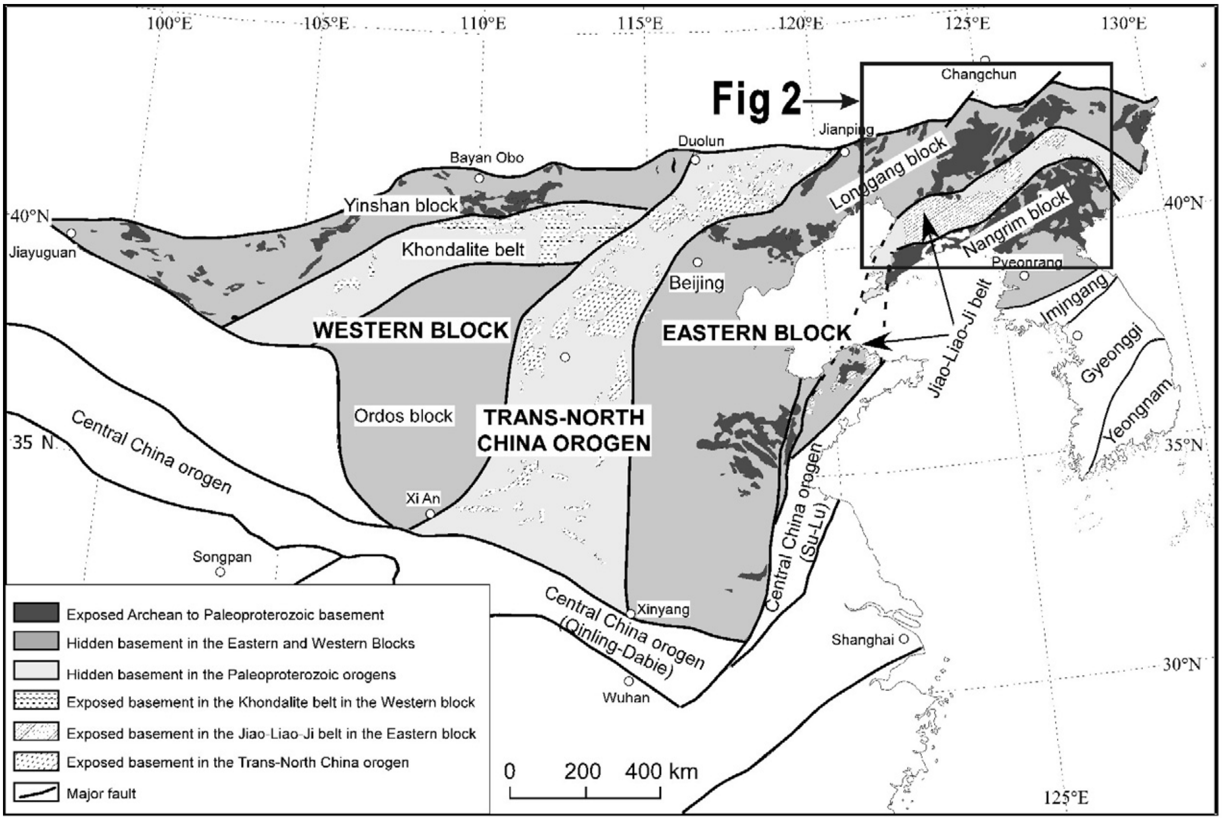

Fig. 1. Archean–Paleoproterozoic terranes of the Sino-Korean Craton (Zhao et al., 2005).

Bureau of Geology and Mineral Resources, 1989). The Fanhe Basin is considered to be a Proterozoic epicratonic embayment with incipient rift affinities (Rui et al., 1991), and is a NE-trending triangular area of about 1800 km^2 bounded by the Tan-Lu Fault to the west, the Hunhe Fault to the south, and the Shahe Fault to the north. The Shahe Fault marks the boundary between the Sino-Korean Craton and the Central Asia Orogenic Belt. In the Fanhe Basin, basaltic dykes, stocks and sills intrude the Liaohe Group and locally the overlying Erdaogou Formation (Wang et al., 1989; Rui et al., 1991). The stratigraphy and lithology of the Liaohe Group in the Fanhe Basin have been reported in detail in previous studies (Wang et al., 1989; Rui et al., 1991; Song and Qiao, 2008) with particular reference to the large Guanmenshan MVT Pb–Zn deposit hosted by this group (Rui et al., 1991; and references therein). In this area, the Liaohe Group, including the lower Daposhan Formation, through the middle Kangzhuangzi Formation, to the upper Guanmenshan Formation, shows a total thickness of 2959 m and consists of, from bottom to top, clastic sediments, shales, and limestones and dolomites (For details see Tang et al., 2011). The Guanmenshan Formation is ~1.5 km thick (Tang et al., 2011) and subdivided into three members. Member 1 is the lowest portion composed of white-gray, silt-bearing, massive, fine-grained dolostones and minor intercalated slates; member 2 is mostly composed of siliceous, pisolitic dolostone, spotted siliceous dolostone, banded algal dolostone, debris-bearing argillaceous dolostone, and stromatolitic micritic dolostone; and member 3 includes bright gray algal dolomite, sand-bearing micritic dolostone, and stromatolitic fine-grained dolostone.

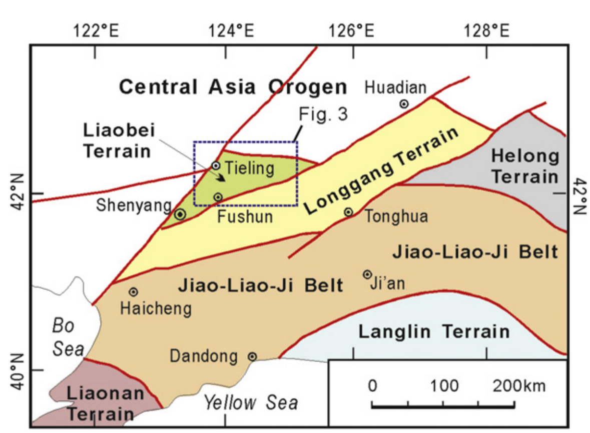

Fig. 2. Tectonic framework of the northeast part of the Sino-Korean Craton (modified after Tang et al., 2011). See Fig. 1 for location.

In spite of the paucity of isotope ages, the Liaohe Group in Liaobei terrain is generally considered to have developed in the interval of 2.3–1.85 Ga (Tang et al., 2011; and references therein). The Guanmenshan Formation of the Liaohe Group shows remarkable positive $\delta^{13}C_{carb}$ anomaly similar to the worldwide positive $\delta^{13}C_{carb}$ excursion in 2.33–2.06 Ga carbonate strata, suggesting that it developed during 2.33–2.06 Ga (Tang et al., 2011).

3. Sampling and analytical methods

The Guanmenshan Formation of the Liaohe Group is dominated by carbonate strata, particularly dolostones, the sequence of which is well exposed along a N—S-trending stratigraphic profile across the Guanmenshan mining area. The formation is named after the Guanmenshan Pb–Zn deposit and is typically exposed in the mining area (Rui et al., 1991) where the stratigraphic profile was measured and systematic sampling carried out for the present study (Fig. 4). Our geological traverse starts at the Lidigou village (124°14.147′E,

Please cite this article in press as: Tang, H.-S., et al., REE geochemistry of carbonates from the Guanmenshan Formation, Liaohe Group, NE Sino-Korean Craton: Implications for seawater compositional change during the Great Oxidation Event. Precambrian Res. (2012), doi:10.1016/j.precamres.2012.02.005

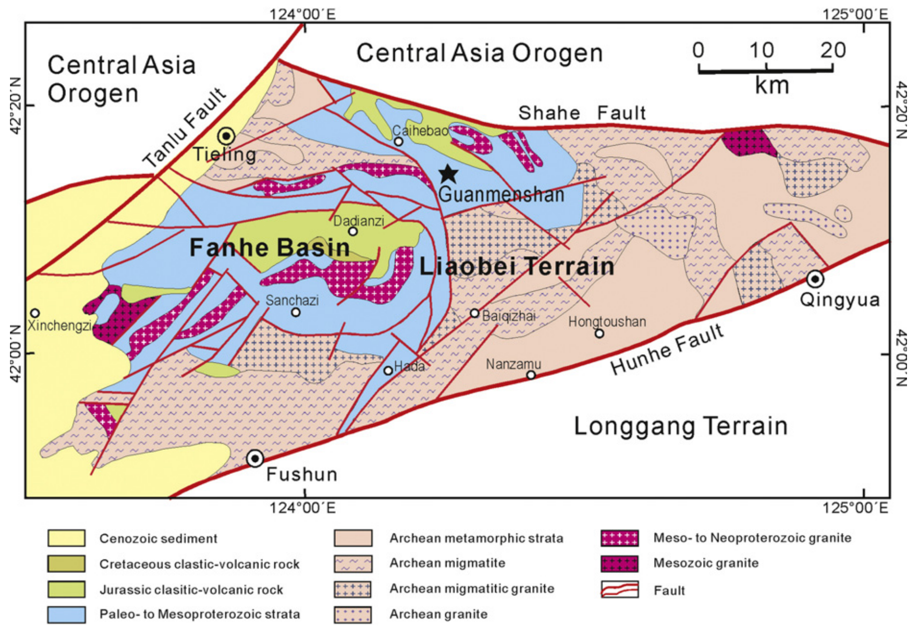

Fig. 3. Simplified geological map of the Fanhe Basin (modified after Liaoning Bureau of Geology and Mineral Resources, 1989). See Fig. 2 for location.

42°13.935′N), continues through the Guanmenshan Pb–Zn Mine (124°14′13″E, 42°12′53″N) (Rui et al., 1991), and culminates at the boundary between the Guanmenshan Formation and Cretaceous volcanic rocks (124°14.458′E, 42°12.790′N), where, close to the Xiaoxigou Pb–Zn Mine (Fig. 4), the strata of the Guanmenshan Formation are fractured and altered. A total of 43 samples were collected from the stratigraphic profile (for samples description details see Table 1 in Tang et al., 2011). Of these, 42 samples are carbonates (mainly dolostones) from the Guanmenshan Formation, only Sample LG006 from a diabase dyke intruding the formation.

Carbonate samples (~0.5–2 kg) were reduced in size using a steel press and a percussion mortar. Small dolostone chips (~1 mm in size, without secondary veins/minerals) were handpicked and ultrasonically cleaned in deionized water and subsequently milled in an agate mortar. Major elements were analyzed by X-ray fluorescence spectrometry (XRF) at the Key Laboratory of Crustal and Orogenic Evolution, Peking University, China, using an ARL ADVANTXP+ X-ray spectrometer. The detection limit for element is around 0.001%, and the precision (1σ) is typically <1% for the major oxide. Acid-soluble trace-element concentrations were analyzed by HR-ICP-MS at State Key Laboratory for Mineral Deposits, Nanjing University, using a Finnigan MAT Element II mass spectrometry. Instrument operating conditions and analytical procedures follow closely those described by Liu et al. (1996). The precision (1σ) is typically <5% for trace elements.

4. Results

The analytical data on major and trace elements are shown in Table 1 and the stratochemical variations are presented in Figs. 5 and 6. Microlithological features of representative samples from the Guanmenshan Formation are shown in Fig. 7. REY (REE + Y) data for all the carbonate rocks are normalized by Post-Archaean Australian Shale (PAAS, subscript SN, McLennan, 1989) and Chondrite (subscript CN, Taylor and McLennan, 1985), respectively. Several element anomalies are defined as follows: $Eu_N/Eu_N^* = Eu_N/(0.67Sm + 0.33Tb)_N$ (Bau and Dulski, 1996; modified by Webb and Kamber, 2000); $La_N/La_N^* = La_N/(3Pr - 2Nd)_N$; $Ce_N/Ce_N^* = Ce_N/(2Pr - Nd)_N$; $Gd_N/Gd_N^* = Gd_N/(2Tb - Dy)_N$ (Bolhar et al., 2004). Depletion of LREE was indicated by Nd_N/Yb_N (Nothdurft et al., 2004) owing to the presence of positive La anomalies and highly variable, negative Ce anomalies in shallow seawater. Pr_N/Sm_N and Sm_N/Yb_N represent the differentiation degree of the LREE/MREE and MREE/HREE, respectively.

The REY patterns are presented in Fig. 8, in which the carbonates are grouped according to their position in the stratigraphic column and lithological features. Group I consists of samples LG001–LG008 collected from the Lidigou area and is located at the bottom of the stratigraphic column (Figs. 4–6). These dolomites (silicified) have constant REE abundances and show flat to slightly MREE-enriched REY patterns, with $Nd_{SN}/Yb_{SN} = 0.94 \pm 0.28$, $Pr_{SN}/Sm_{SN} = 1.02 \pm 0.15$

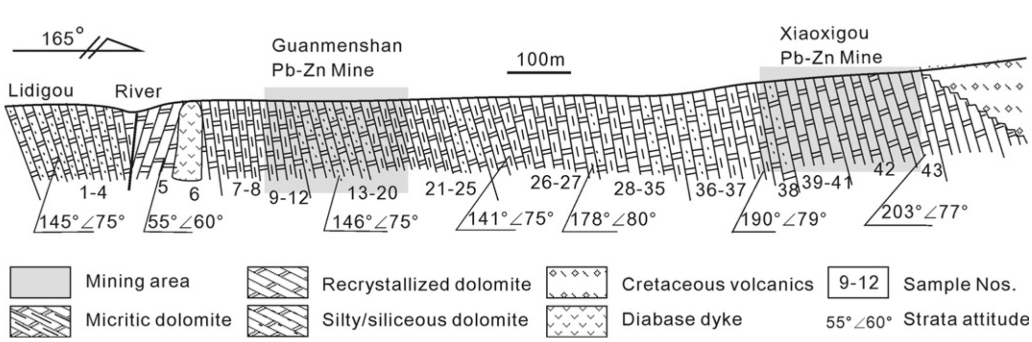

Fig. 4. Stratigraphic profile of the Guanmenshan Formation showing sample locations.

Please cite this article in press as: Tang, H.-S., et al., REE geochemistry of carbonates from the Guanmenshan Formation, Liaohe Group, NE Sino-Korean Craton: Implications for seawater compositional change during the Great Oxidation Event. Precambrian Res. (2012), doi:10.1016/j.precamres.2012.02.005

Table 1
Major (wt.%) and trace (ppm) element contents in carbonates from the Guanmenshan Formation, Liaohe Group.

Sample	Height (m)	Al_2O_3	CaO	$Fe_2O_3^T$	K_2O	MgO	MnO	Na_2O	P_2O_5	SiO_2	TiO_2	LOI	TOL
LG001	8	0.42	23.02	0.05	<0.01	14.93	0.015	0.26	0.03	32.21	<0.001	29.04	99.98
LG002	28	0.49	27.07	0.12	<0.01	19.49	0.023	0.29	0.043	13.14	<0.001	39.31	99.98
LG003	46	0.44	26.74	0.11	<0.01	19.47	0.034	0.29	0.037	14.88	<0.001	37.99	99.98
LG004	203.2	0.49	28.42	0.1	<0.01	20.88	0.028	0.28	0.033	5.42	<0.001	44.32	99.98
LG005	266.3	0.63	28.57	1.32	<0.01	19.51	0.136	0.28	0.06	4.84	0.005	44.62	99.96
LG007	273.1	0.64	27.99	0.67	<0.01	20.39	0.023	0.28	0.065	8.32	<0.001	41.61	99.98
LG008	279.9	0.55	28.27	0.05	<0.01	21.28	0.02	0.3	0.052	5.75	<0.001	43.7	99.98
LG009	300.4	0.42	28.72	0.07	<0.01	21.52	0.018	0.28	0.047	2.46	<0.001	46.44	99.99
LG010	303.8	0.7	28.66	0.14	<0.01	21.65	0.015	0.31	0.077	2.31	0.001	45.92	99.78
LG011	320.9	0.63	28.81	0.11	<0.01	21.16	0.015	0.3	0.075	2.84	<0.001	45.98	99.92
LG012	396.2	0.43	28.45	0.22	<0.01	21.35	0.027	0.31	0.062	4.61	<0.001	44.52	99.98
LG013	409.9	0.47	19.32	0.1	<0.01	12.35	0.031	0.24	0.018	45	<0.001	22.47	99.98
LG014	424.1	0.39	25.33	0.08	<0.01	17.09	0.017	0.27	0.025	23.13	<0.001	33.66	99.98
LG015	431.2	0.36	19.2	0.06	<0.01	10.32	0.016	0.21	0.016	47.61	<0.001	22.19	99.99
LG016	454	0.4	27.8	0.13	<0.01	19.95	0.023	0.28	0.017	10.97	<0.001	40.41	99.98
LG017	488	0.41	26.28	0.1	<0.01	18.71	0.023	0.28	0.038	17.93	<0.001	36.22	99.98
LG018	516.4	0.39	19.74	0.13	<0.01	10.57	0.019	0.22	0.036	46.64	<0.001	22.25	99.99
LG019	530.6	0.44	29.18	0.22	<0.01	21.28	0.027	0.29	0.016	1.95	<0.001	46.58	99.98
LG020	551.9	0.42	28.85	0.22	<0.01	21.71	0.032	0.28	0.039	1.89	<0.001	46.54	99.98
LG021	559	0.42	29	0.33	<0.01	20.91	0.034	0.29	0.072	3.21	<0.001	45.71	99.98
LG022	630	0.39	28.97	0.32	<0.01	21.49	0.034	0.29	0.05	2.04	<0.001	46.4	99.98
LG023	637.1	0.93	28.19	0.73	0.05	19.94	0.048	0.29	0.478	6.1	0.125	43.06	99.96
LG024	658.4	0.4	27.28	0.31	<0.01	20.04	0.037	0.27	0.054	11.73	<0.001	39.85	99.98
LG025	672.6	0.45	27.93	0.46	<0.01	19.91	0.128	0.28	0.172	8.91	<0.001	41.74	99.98
LG026	693.9	0.41	28.65	0.45	<0.01	20.54	0.069	0.29	0.196	4.14	<0.001	45.23	99.98
LG027	833	0.52	28.85	0.27	<0.01	21.23	0.044	0.28	0.303	2.38	<0.001	46.09	99.98
LG028	848.5	0.48	28.85	0.26	<0.01	21.76	0.04	0.31	0.036	2.51	<0.001	45.73	99.98
LG029	864	0.52	28.54	0.14	<0.01	21.33	0.024	0.29	0.167	4.01	0.002	44.94	99.98
LG030	887.2	0.44	28.84	0.08	<0.01	21.94	0.028	0.3	0.013	2.71	<0.001	45.64	99.98
LG031	918.1	0.62	27.68	0.33	<0.01	20.45	0.052	0.29	0.119	8.89	<0.001	41.54	99.97
LG032	933.6	0.38	28.05	0.05	<0.01	20.99	0.021	0.3	0.045	7.32	<0.001	42.84	99.99
LG033	956.8	0.39	27.01	0.11	<0.01	19.34	0.025	0.28	0.041	14.71	<0.001	38.08	99.98
LG034	968.5	0.45	28.17	0.15	<0.01	21.3	0.034	0.31	0.021	4.92	<0.001	44.62	99.98
LG035	986.1	0.4	27.78	0.09	<0.01	21.22	0.023	0.3	0.046	8.23	<0.001	41.89	99.98
LG036	1062.4	0.57	27.35	0.27	<0.01	20.09	0.025	0.28	0.043	11.24	<0.001	40.11	99.98
LG037	1138.7	1.18	27.76	0.33	0.18	20.63	0.012	0.29	0.039	5.29	0.026	44.23	99.96
LG038	1150.4	0.84	26.68	0.6	0.02	18.12	0.023	0.27	0.031	14.57	0.024	38.81	99.98
LG039	1162.1	0.4	28.82	0.4	<0.01	21.25	0.028	0.28	0.018	2.13	<0.001	46.64	99.96
LG040	1173.8	0.39	28.68	0.55	<0.01	21.34	0.038	0.29	0.025	2.22	<0.001	46.42	99.96
LG041	1185.5	0.48	29	0.23	<0.01	21.65	0.017	0.29	0.031	1.68	<0.001	46.59	99.97
LG042	1414.4	0.39	29.05	0.96	<0.01	20.31	0.054	0.29	0.053	3.27	<0.001	45.59	99.96
LG043	1469.5	0.47	28.59	0.42	<0.01	20.39	0.04	0.29	0.058	4.83	<0.001	44.88	99.97

Sample	Li	Be	Sc	Ti	V	Cr	Mn	Co	Ni	Cu	Zn	Ga	Rb	Sr
LG001	0.581	0.039	0.275	9.073	3.432	72.761	247.528	1.014	29.966	4.618	12.614	0.146	0.241	53.511
LG002	1.109	0.045	0.435	33.482	4.040	18.265	186.997	0.619	6.725	2.435	10.745	0.248	0.731	73.960
LG003	0.959	0.083	0.465	14.302	3.669	46.592	205.771	0.699	17.057	2.738	6.948	0.185	0.430	76.727
LG004	2.053	0.068	0.805	24.994	3.353	81.291	180.047	0.866	28.631	3.249	11.507	0.213	0.776	127.181
LG005	0.8002	0.123	0.9227	72.2246	12.4644	33.174	900.387	3.643	12.8279	5.4009	51.997	0.5939	1.1267	136.1943
LG007	1.388	0.097	0.631	56.636	11.601	45.083	155.581	1.526	21.630	3.026	52.284	0.398	1.054	61.390
LG008	1.244	0.062	0.616	46.331	2.686	14.852	120.008	0.359	5.679	7.360	65.759	0.216	0.945	50.114
LG009	0.972	0.025	0.576	13.672	1.742	12.004	127.770	0.429	75.699	1.586	70.196	0.098	0.439	47.431
LG010	1.328	0.048	0.754	53.088	3.248	18.126	102.751	0.605	8.115	6.077	130.138	0.274	1.446	99.036
LG011	1.402	0.097	0.761	51.785	3.369	13.349	100.382	0.588	3.419	3.282	80.711	0.287	1.637	82.150
LG012	1.242	0.054	0.539	18.938	3.412	110.891	169.050	1.126	70.604	4.219	49.346	0.152	0.499	66.279
LG013	0.605	0.022	0.203	7.492	2.837	32.230	168.103	0.404	13.142	1.885	62.414	0.155	0.444	46.071
LG014	0.610	0.047	0.253	7.293	2.234	16.137	133.402	0.433	4.043	2.126	61.250	0.080	0.199	42.909
LG015	0.356	0.019	0.119	3.978	2.767	14.773	99.492	0.225	3.301	1.451	7.455	0.042	0.101	39.290
LG016	0.719	0.024	0.308	9.060	2.659	90.320	146.534	0.627	20.233	3.298	26.219	0.104	0.193	48.299
LG017	0.552	0.026	0.265	6.575	2.033	15.133	132.788	0.432	6.179	1.799	13.596	0.064	0.090	49.481
LG018	0.386	0.029	0.115	6.899	2.689	19.313	104.458	0.262	7.397	1.357	12.449	0.048	0.063	36.006
LG019	0.725	0.032	0.383	9.336	4.476	9.675	158.470	0.515	6.991	1.738	17.113	0.067	0.217	65.565
LG020	0.879	0.042	0.560	12.971	1.628	8.432	185.526	0.454	2.768	1.798	55.969	0.118	0.260	55.007
LG021	0.753	0.039	0.559	18.736	6.375	15.174	223.372	0.896	5.664	2.290	96.397	0.121	0.311	77.313
LG022	0.904	0.039	0.553	12.628	5.409	12.957	208.856	0.875	5.511	2.004	135.034	0.122	0.283	61.231
LG023	1.458	0.121	1.643	785.566	26.867	19.387	283.599	2.137	9.304	7.026	33.314	0.813	2.229	224.456
LG024	0.632	0.036	0.449	20.320	7.068	12.681	231.353	0.539	2.801	2.283	26.646	0.169	0.241	51.500
LG025	0.915	0.043	0.447	20.646	5.073	22.286	823.304	0.622	8.671	2.155	24.283	0.397	0.406	46.925
LG026	1.014	0.048	0.467	12.041	6.644	9.128	441.124	0.576	2.358	1.771	30.832	0.207	0.251	60.185
LG027	0.833	0.070	0.508	49.416	7.144	18.192	275.713	0.544	5.916	1.910	21.997	0.271	0.806	62.956
LG028	1.193	0.047	0.507	59.521	6.321	18.320	250.825	0.691	4.559	2.173	23.265	0.225	0.671	72.753
LG029	1.230	0.104	0.631	71.372	8.408	10.453	160.486	0.806	3.022	2.839	31.132	0.276	0.887	90.705
LG030	1.064	0.063	0.432	22.063	9.933	13.362	166.428	0.683	4.489	2.114	8.596	0.182	0.459	85.088
LG031	1.628	0.074	0.625	47.391	11.273	12.112	310.629	0.848	4.471	3.162	59.145	0.363	1.104	69.820
LG032	0.560	0.021	0.409	5.636	2.957	60.117	131.009	0.592	12.248	1.771	40.481	0.082	0.116	42.922

Please cite this article in press as: Tang, H.-S., et al., REE geochemistry of carbonates from the Guanmenshan Formation, Liaohe Group, NE Sino-Korean Craton: Implications for seawater compositional change during the Great Oxidation Event. Precambrian Res. (2012), doi:10.1016/j.precamres.2012.02.005

Table 1 (*Continued*)

Sample	Li	Be	Sc	Ti	V	Cr	Mn	Co	Ni	Cu	Zn	Ga	Rb	Sr
LG033	0.584	0.036	0.354	5.916	5.233	11.144	140.963	0.721	2.752	2.044	50.620	0.084	0.103	60.010
LG034	1.063	0.050	0.504	16.245	8.554	10.356	199.723	0.793	3.411	3.848	75.229	0.236	0.634	92.422
LG035	0.588	0.028	0.421	10.782	6.907	12.622	149.386	0.614	3.183	2.365	45.309	0.092	0.287	60.979
LG036	1.288	0.106	0.406	55.780	16.852	352.551	193.739	2.878	129.900	5.171	101.830	0.390	1.264	91.416
LG037	2.615	0.138	1.164	176.654	8.027	18.298	77.458	0.941	7.959	11.264	51.209	1.079	5.472	125.247
LG038	0.923	0.106	0.961	163.095	25.266	17.698	143.204	1.325	8.025	2.862	24.904	0.646	2.492	84.429
LG039	0.771	0.044	0.584	17.228	3.675	31.337	177.437	1.062	13.858	2.565	51.619	0.219	0.309	156.743
LG040	1.132	0.121	0.583	22.688	5.356	15.889	253.130	1.381	23.462	2.896	82.645	0.147	0.178	123.620
LG041	0.944	0.126	0.648	24.868	9.403	12.518	348.063	0.978	7.093	5.851	106.695	0.250	0.276	103.899
LG042	1.248	0.085	0.605	28.439	4.116	11.071	112.871	0.833	5.128	1.345	35.195	0.242	0.595	126.432
LG043	1.366	0.090	0.554	32.835	7.652	14.195	246.675	0.740	24.095	4.190	28.533	0.239	0.575	99.810

Sample	Zr	Nb	Mo	Cd	Sn	Cs	Ba	Hf	Ta	W	Pb	Bi	Th	U
LG001	0.610	0.104	4.827	0.147	0.737	0.018	11.290	0.012	0.035	0.560	2.622	0.019	0.025	0.226
LG002	1.931	0.225	2.390	0.284	0.217	0.101	14.007	0.039	0.030	0.233	11.773	0.035	0.113	0.222
LG003	0.925	0.098	4.844	0.156	0.364	0.047	22.919	0.018	0.060	0.390	6.752	0.026	0.069	0.202
LG004	1.524	0.130	3.597	0.122	0.457	0.041	28.176	0.038	0.029	0.335	5.212	0.023	0.143	0.256
LG005	2.0474	0.1364	2.4271	0.8041	0.5019	0.0599	40.1028	0.0487	0.0479	0.2794	51.926	0.099	0.1058	0.1468
LG007	3.410	0.216	5.261	0.058	0.243	0.017	28.429	0.065	0.041	0.577	6.163	0.084	0.162	0.316
LG008	3.996	0.188	1.567	0.085	0.548	0.025	96.331	0.092	0.037	0.169	3.145	0.018	0.150	0.233
LG009	0.653	0.047	1.849	0.144	0.156	0.013	19.152	0.017	0.027	0.122	4.199	0.017	0.061	0.136
LG010	2.259	0.146	2.370	0.209	0.279	0.051	2058.051	0.062	0.037	0.362	4.197	0.018	0.207	0.248
LG011	2.508	0.188	1.280	0.155	0.353	0.060	628.215	0.051	0.042	0.191	4.309	0.035	0.226	0.273
LG012	0.808	0.125	5.196	0.080	0.515	0.123	20.424	0.013	0.030	0.527	2.770	0.023	0.072	0.235
LG013	0.597	0.043	1.947	0.133	0.177	0.007	28.534	0.010	0.024	0.208	1.644	0.012	0.007	0.128
LG014	0.452	0.072	1.427	0.178	0.215	0.025	15.040	0.004	0.026	0.196	3.661	0.029	0.035	0.189
LG015	0.278	0.028	2.227	0.059	0.175	0.006	10.310	0.003	0.024	0.186	1.384	0.015	0.017	0.212
LG016	0.602	0.090	6.937	0.310	0.533	0.008	9.240	0.012	0.031	0.310	2.707	0.023	0.031	0.206
LG017	0.394	0.047	1.774	0.118	0.210	0.006	6.307	0.008	0.028	0.177	2.349	0.014	0.019	0.168
LG018	0.549	0.040	1.749	0.043	0.203	<0.01	3.876	0.007	0.027	0.178	1.212	0.012	0.019	0.185
LG019	0.665	0.071	1.402	0.105	0.180	0.015	4.397	0.012	0.031	0.121	6.852	0.028	0.042	0.200
LG020	0.673	0.045	0.794	0.112	0.181	0.006	9.431	0.015	0.032	0.145	4.563	0.031	0.049	0.216
LG021	0.965	0.065	2.875	0.194	0.262	0.016	6.992	0.025	0.039	0.238	11.332	0.027	0.053	0.274
LG022	0.647	0.049	2.361	0.095	0.161	0.008	6.123	0.011	0.104	0.126	6.903	0.047	0.030	0.225
LG023	10.273	0.634	1.800	0.266	0.550	0.065	37.540	0.225	0.066	1.477	16.716	0.058	0.496	1.130
LG024	0.826	0.044	1.546	0.122	0.301	0.015	8.759	0.017	0.024	0.165	9.984	0.033	0.026	0.363
LG025	2.332	0.098	3.386	0.302	0.307	0.039	12.511	0.057	0.105	0.289	11.095	0.045	0.062	0.378
LG026	2.737	0.048	1.264	0.192	0.150	0.019	9.672	0.054	0.024	0.126	13.014	0.029	0.054	0.412
LG027	3.718	0.187	1.745	0.084	0.256	0.054	9.079	0.097	0.042	0.256	3.630	0.021	0.126	0.609
LG028	1.325	0.259	3.372	0.351	0.222	0.028	67.036	0.029	0.039	0.338	10.562	0.030	0.085	0.294
LG029	4.360	0.238	1.054	0.272	0.314	0.033	73.585	0.103	0.040	0.182	10.441	0.034	0.326	0.845
LG030	1.348	0.083	3.106	0.057	0.134	0.012	55.973	0.023	0.026	0.160	2.618	0.013	0.058	1.092
LG031	3.266	0.158	2.194	0.106	0.254	0.030	133.140	0.077	0.038	0.145	4.548	0.032	0.142	0.676
LG032	1.064	0.067	9.065	0.106	0.211	0.011	11.373	0.022	0.025	0.326	4.413	0.019	0.009	0.240
LG033	0.701	0.054	1.635	0.104	0.209	0.006	11.231	0.008	0.031	0.206	4.602	0.016	0.009	0.442
LG034	2.249	0.062	1.953	0.273	0.324	0.048	41.782	0.032	0.032	0.159	11.981	0.109	0.087	0.510
LG035	0.747	0.091	4.724	0.163	0.237	0.015	9.817	0.012	0.036	0.224	10.590	0.030	0.051	0.432
LG036	3.372	0.328	24.947	0.218	0.673	0.035	25.410	0.083	0.039	0.711	7.621	0.029	0.206	0.559
LG037	9.282	0.503	3.493	0.109	0.259	0.108	121.273	0.248	0.070	0.306	5.539	0.040	0.678	0.429
LG038	2.664	0.218	5.024	0.144	0.256	0.424	17.509	0.056	0.040	0.538	7.704	0.012	0.064	0.613
LG039	0.884	0.061	2.010	0.750	0.186	0.028	8.734	0.013	0.034	0.171	36.300	0.013	0.049	0.127
LG040	1.362	0.116	3.005	1.117	0.195	0.013	7.080	0.025	0.029	0.264	63.557	0.031	0.048	0.259
LG041	3.855	0.107	1.138	0.862	0.210	0.016	11.598	0.061	0.029	0.367	78.768	0.017	0.056	1.196
LG042	1.730	0.101	2.675	0.813	0.274	0.038	19.467	0.042	0.044	0.214	41.208	0.009	0.134	0.282
LG043	2.366	0.130	1.004	0.280	0.215	0.031	14.200	0.050	0.042	0.128	20.999	0.026	0.111	0.552

Sample	Y	La	Ce	Pr	Nd	Sm	Eu	Gd	Tb	Dy	Ho	Er	Tm	Yb	Lu
LG001	0.190	0.157	0.295	0.029	0.074	0.025	0.005	0.027	0.004	0.018	0.006	0.019	0.002	0.015	0.002
LG002	0.462	0.404	0.881	0.093	0.326	0.075	0.016	0.063	0.008	0.052	0.011	0.038	0.006	0.041	0.005
LG003	0.433	0.387	0.889	0.095	0.374	0.050	0.016	0.058	0.008	0.063	0.013	0.039	0.005	0.033	0.003
LG004	0.388	0.790	1.458	0.138	0.522	0.084	0.022	0.074	0.009	0.057	0.014	0.040	0.006	0.032	0.004
LG005	1.0713	1.1921	2.2543	0.2158	0.8496	0.1317	0.0621	0.1808	0.0232	0.1527	0.0328	0.107	0.0181	0.0891	0.015
LG007	0.598	0.535	1.152	0.112	0.424	0.066	0.025	0.095	0.012	0.084	0.016	0.039	0.008	0.034	0.007
LG008	0.596	0.442	0.987	0.100	0.412	0.061	0.018	0.087	0.013	0.065	0.015	0.047	0.007	0.049	0.006
LG009	0.270	0.323	0.719	0.062	0.249	0.031	0.013	0.043	0.006	0.029	0.010	0.023	0.003	0.019	0.004
LG010	0.472	0.577	1.247	0.135	0.473	0.097	0.132	0.160	0.011	0.056	0.018	0.046	0.005	0.044	0.006
LG011	0.589	0.651	1.380	0.145	0.509	0.098	0.054	0.125	0.013	0.083	0.018	0.059	0.008	0.051	0.007
LG012	0.295	0.400	0.827	0.079	0.326	0.069	0.021	0.061	0.008	0.040	0.008	0.028	0.004	0.023	0.002
LG013	0.236	0.086	0.221	0.025	0.066	0.013	0.008	0.019	0.003	0.022	0.007	0.025	0.002	0.018	0.002
LG014	0.143	0.177	0.329	0.030	0.098	0.023	0.010	0.026	0.002	0.010	0.002	0.010	0.001	0.008	0.001
LG015	0.066	0.071	0.178	0.014	0.057	0.014	0.004	0.018	0.001	0.005	0.001	0.003	0.001	0.008	0.001
LG016	0.173	0.136	0.302	0.031	0.088	0.018	0.009	0.020	0.003	0.019	0.004	0.013	0.001	0.012	0.001
LG017	0.177	0.149	0.301	0.028	0.095	0.019	0.010	0.021	0.003	0.015	0.004	0.015	0.001	0.007	0.001
LG018	0.270	0.156	0.331	0.035	0.113	0.012	0.014	0.026	0.003	0.028	0.007	0.019	0.003	0.015	0.002
LG019	0.295	0.333	0.578	0.059	0.200	0.032	0.017	0.034	0.004	0.028	0.008	0.024	0.003	0.015	0.002

Table 1 (*Continued*)

Sample	Y	La	Ce	Pr	Nd	Sm	Eu	Gd	Tb	Dy	Ho	Er	Tm	Yb	Lu
LG020	0.324	0.318	0.599	0.061	0.220	0.031	0.021	0.041	0.005	0.033	0.008	0.019	0.003	0.013	0.003
LG021	0.532	0.370	0.757	0.082	0.311	0.048	0.025	0.078	0.009	0.055	0.013	0.042	0.005	0.034	0.004
LG022	0.466	0.341	0.698	0.078	0.252	0.037	0.022	0.064	0.008	0.041	0.011	0.036	0.004	0.029	0.008
LG023	3.142	0.982	2.642	0.372	1.921	0.539	0.089	0.525	0.073	0.460	0.101	0.294	0.035	0.222	0.029
LG024	0.624	0.251	0.470	0.055	0.215	0.043	0.023	0.054	0.008	0.057	0.013	0.043	0.006	0.035	0.004
LG025	0.981	0.610	1.059	0.146	0.561	0.119	0.035	0.122	0.014	0.109	0.028	0.082	0.010	0.059	0.008
LG026	0.730	0.572	1.068	0.107	0.387	0.072	0.034	0.090	0.010	0.075	0.017	0.052	0.008	0.035	0.007
LG027	1.108	0.576	1.076	0.107	0.385	0.082	0.040	0.103	0.013	0.092	0.028	0.086	0.008	0.068	0.008
LG028	1.970	0.431	1.115	0.155	0.616	0.133	0.038	0.156	0.024	0.161	0.050	0.147	0.022	0.120	0.017
LG029	3.147	0.715	1.256	0.172	0.821	0.146	0.043	0.227	0.028	0.229	0.068	0.236	0.029	0.181	0.023
LG030	1.278	0.302	0.514	0.068	0.272	0.049	0.017	0.060	0.008	0.073	0.026	0.085	0.012	0.075	0.009
LG031	2.521	0.766	1.621	0.209	0.875	0.184	0.058	0.210	0.028	0.223	0.064	0.177	0.028	0.132	0.020
LG032	0.336	0.175	0.288	0.030	0.102	0.025	0.009	0.036	0.004	0.024	0.007	0.020	0.003	0.015	0.002
LG033	0.821	0.199	0.365	0.041	0.124	0.024	0.013	0.039	0.006	0.044	0.015	0.042	0.007	0.042	0.005
LG034	0.722	0.449	0.798	0.097	0.333	0.057	0.024	0.066	0.011	0.076	0.017	0.057	0.006	0.044	0.006
LG035	0.990	0.459	0.800	0.087	0.300	0.058	0.021	0.066	0.008	0.069	0.021	0.061	0.011	0.055	0.009
LG036	1.656	0.756	1.505	0.194	0.762	0.136	0.038	0.148	0.022	0.150	0.042	0.121	0.016	0.110	0.013
LG037	1.210	1.901	4.281	0.444	1.645	0.298	0.071	0.308	0.036	0.241	0.051	0.153	0.019	0.148	0.020
LG038	0.873	0.434	0.987	0.121	0.577	0.124	0.043	0.138	0.017	0.118	0.025	0.072	0.013	0.077	0.009
LG039	0.347	0.244	0.532	0.060	0.224	0.042	0.017	0.051	0.007	0.050	0.010	0.030	0.004	0.024	0.003
LG040	0.204	0.258	0.487	0.046	0.179	0.038	0.008	0.033	0.003	0.031	0.007	0.019	0.002	0.013	0.002
LG041	0.634	0.676	1.230	0.126	0.437	0.074	0.065	0.119	0.010	0.077	0.018	0.057	0.007	0.047	0.005
LG042	0.467	0.356	0.831	0.089	0.320	0.084	0.018	0.066	0.010	0.059	0.016	0.043	0.005	0.045	0.003
LG043	0.484	0.376	0.739	0.076	0.264	0.051	0.023	0.068	0.011	0.063	0.015	0.048	0.006	0.044	0.003

Sample	$\sum$REE	Y/Ho	Mn/Sr	Sm/Yb	Eu/Sm	Nd_{CN}/Yb_{CN}	Sm_{CN}/Yb_{CN}	Eu_{CN}/Sm_{CN}	$Ce_{CN}/Ce_{CN}{}^*$	$Eu_{CN}/Eu_{CN}{}^*$
LG001	0.676	32.8	4.63	1.67	0.18	1.74	1.79	0.48	0.99	0.56
LG002	2.019	40.5	2.53	1.83	0.21	2.78	1.97	0.57	1.03	0.7
LG003	2.034	34.6	2.68	1.55	0.31	4.01	1.66	0.83	1.08	0.96
LG004	3.249	28.1	1.42	2.63	0.27	5.7	2.83	0.7	1.19	0.87
LG005	5.3243	32.662	6.61	1.48	0.47	3.33	1.59	1.25	1.2	1.39
LG007	2.608	36.9	2.53	1.96	0.38	4.39	2.11	1	1.16	1.11
LG008	2.308	39.7	2.39	1.23	0.3	2.93	1.33	0.79	1.17	0.84
LG009	1.532	27.3	2.69	1.64	0.44	4.66	1.76	1.16	1.37	1.25
LG010	3.008	26.8	1.04	2.22	1.37	3.79	2.38	3.63	1	4.45
LG011	3.201	32.7	1.22	1.92	0.55	3.46	2.06	1.46	1.03	1.73
LG012	1.898	36.9	2.55	2.96	0.3	4.85	3.18	0.8	1.24	0.98
LG013	0.516	35.7	3.65	0.71	0.65	1.3	0.77	1.74	0.86	1.83
LG014	0.727	64.8	3.11	2.8	0.44	4.24	3.01	1.17	1.14	1.48
LG015	0.374	54.9	2.53	1.75	0.25	2.47	1.88	0.66	1.56	0.83
LG016	0.657	48.1	3.03	1.42	0.53	2.46	1.52	1.4	0.98	1.61
LG017	0.668	43.0	2.68	2.76	0.53	4.87	2.97	1.4	1.15	1.56
LG018	0.763	36.9	2.9	0.8	1.17	2.65	0.86	3.1	0.98	3.17
LG019	1.336	35.1	2.42	2.16	0.53	4.71	2.32	1.39	1.05	1.65
LG020	1.373	42.6	3.37	2.33	0.69	5.81	2.51	1.83	1.09	2.09
LG021	1.830	42.6	2.89	1.4	0.53	3.2	1.5	1.4	1.05	1.53
LG022	1.628	43.5	3.41	1.29	0.6	3.08	1.39	1.59	0.94	1.64
LG023	8.282	31.2	1.26	2.43	0.16	3.02	2.61	0.44	1.01	0.52
LG024	1.275	47.6	4.45	1.23	0.53	2.17	1.33	1.4	1	1.51
LG025	2.961	34.5	17.55	2.01	0.3	3.31	2.16	0.79	0.82	0.95
LG026	2.534	42.5	7.33	2.05	0.48	3.87	2.21	1.27	1.1	1.47
LG027	2.672	39.6	4.38	1.22	0.49	1.99	1.31	1.29	1.11	1.48
LG028	3.186	39.5	3.45	1.11	0.29	1.8	1.2	0.77	0.83	0.84
LG029	4.175	46.1	1.77	0.81	0.3	1.58	0.87	0.79	0.97	0.86
LG030	1.572	49.5	1.96	0.66	0.35	1.27	0.71	0.94	0.87	1.05
LG031	4.593	39.5	4.45	1.4	0.31	2.32	1.5	0.83	0.93	0.95
LG032	0.739	51.7	3.05	1.69	0.36	2.42	1.81	0.95	1.03	1.09
LG033	0.965	56.6	2.35	0.57	0.55	1.02	0.62	1.45	0.91	1.5
LG034	2.041	41.5	2.16	1.29	0.41	2.62	1.39	1.09	0.88	1.19
LG035	2.025	47.6	2.45	1.07	0.35	1.91	1.14	0.94	0.99	1.1
LG036	4.013	39.5	2.12	1.24	0.28	2.42	1.33	0.74	0.9	0.84
LG037	9.616	24.0	0.62	2.01	0.24	3.87	2.15	0.64	1.07	0.77
LG038	2.756	34.6	1.7	1.6	0.35	2.6	1.72	0.92	1.08	1.08
LG039	1.297	34.7	1.13	1.72	0.41	3.23	1.85	1.1	0.99	1.25
LG040	1.125	30.0	2.05	2.83	0.22	4.68	3.04	0.58	1.2	0.75
LG041	2.947	35.2	3.35	1.59	0.88	3.27	1.7	2.34	1.05	2.73
LG042	1.942	29.9	0.89	1.88	0.21	2.49	2.02	0.56	1.03	0.69
LG043	1.786	32.3	2.47	1.18	0.45	2.11	1.27	1.19	1.06	1.26

Sample	Nd_{SN}/Yb_{SN}	Sm_{SN}/Yb_{SN}	Pr_{SN}/Sm_{SN}	$La_{SN}/La_{SN}{}^*$	$Ce_{SN}/Ce_{SN}{}^*$	$Pr_{SN}/Pr_{SN}{}^*$	$Gd_{SN}/Gd_{SN}{}^*$	$Eu_{SN}/Eu_{SN}{}^*$
LG001	0.41	0.85	0.72	0.77	0.87	1.1	1.29	0.93
LG002	0.66	0.93	0.78	0.86	0.97	1.02	1.16	1.18
LG003	0.96	0.79	1.18	1	1.07	0.97	1.3	1.56
LG004	1.36	1.34	1.03	1.28	1.15	0.93	1.25	1.48
LG005	0.79	0.75	1.03	1.35	1.19	0.92	1.39	2.23
LG007	1.05	1	1.06	1.08	1.13	0.94	1.45	1.79

Please cite this article in press as: Tang, H.-S., et al., REE geochemistry of carbonates from the Guanmenshan Formation, Liaohe Group, NE Sino-Korean Craton: Implications for seawater compositional change during the Great Oxidation Event. Precambrian Res. (2012), doi:10.1016/j.precamres.2012.02.005

Table 1 (*Continued*)

Sample	Nd_{SN}/Yb_{SN}	Sm_{SN}/Yb_{SN}	Pr_{SN}/Sm_{SN}	La_{SN}/La_{SN}^*	Ce_{SN}/Ce_{SN}^*	Pr_{SN}/Pr_{SN}^*	Gd_{SN}/Gd_{SN}^*	Eu_{SN}/Eu_{SN}^*
LG008	0.7	0.63	1.04	1.19	1.18	0.92	1.28	1.32
LG009	1.11	0.83	1.27	1.35	1.37	0.85	1.31	1.97
LG010	0.9	1.13	0.88	0.84	0.94	1.03	2.29	7.55
LG011	0.83	0.97	0.93	0.89	0.97	1.01	1.57	2.87
LG012	1.16	1.5	0.72	1.36	1.25	0.9	1.18	1.65
LG013	0.31	0.36	1.23	0.5	0.76	1.19	1.32	2.86
LG014	1.01	1.42	0.84	1.04	1.05	0.97	1.76	2.55
LG015	0.59	0.89	0.61	1.46	1.59	0.79	1.84	1.42
LG016	0.59	0.72	1.09	0.69	0.88	1.08	1.27	2.63
LG017	1.16	1.4	0.93	1	1.07	0.96	1.15	2.52
LG018	0.63	0.41	1.85	0.78	0.91	1.06	1.77	4.89
LG019	1.12	1.1	1.15	1.07	0.98	1.01	1.31	2.73
LG020	1.38	1.19	1.23	1.1	1.04	0.98	1.46	3.41
LG021	0.76	0.71	1.08	1.03	1.02	0.99	1.59	2.44
LG022	0.73	0.66	1.32	0.78	0.86	1.09	1.44	2.55
LG023	0.72	1.23	0.43	1.95	1.2	0.94	1.19	0.85
LG024	0.52	0.63	0.8	1.12	0.98	1.01	1.19	2.4
LG025	0.79	1.02	0.78	0.96	0.8	1.11	1.37	1.61
LG026	0.92	1.04	0.93	1.12	1.05	0.97	1.46	2.42
LG027	0.47	0.62	0.82	1.11	1.06	0.97	1.4	2.42
LG028	0.43	0.57	0.73	0.69	0.83	1.09	1.15	1.34
LG029	0.38	0.41	0.74	1.9	1.08	0.97	1.49	1.36
LG030	0.3	0.34	0.87	1.1	0.87	1.07	1.25	1.69
LG031	0.55	0.71	0.71	1.04	0.95	1.02	1.27	1.55
LG032	0.58	0.86	0.76	1.11	0.96	1.02	1.6	1.77
LG033	0.24	0.29	1.06	0.8	0.82	1.12	1.35	2.33
LG034	0.62	0.66	1.06	0.89	0.83	1.1	1.11	1.89
LG035	0.46	0.54	0.93	1.02	0.93	1.04	1.36	1.82
LG036	0.58	0.63	0.9	0.95	0.88	1.06	1.16	1.36
LG037	0.92	1.02	0.94	0.93	1.03	0.98	1.35	1.29
LG038	0.62	0.81	0.61	1.61	1.2	0.93	1.33	1.78
LG039	0.77	0.88	0.9	0.89	0.96	1.02	1.33	2.04
LG040	1.12	1.44	0.77	1.31	1.18	0.92	1.53	1.32
LG041	0.78	0.81	1.07	1.03	0.98	1.01	1.9	4.51
LG042	0.59	0.95	0.66	0.83	0.98	1.01	1.05	1.16
LG043	0.5	0.6	0.92	0.97	1	1	1.17	1.97

and $Sm_{SN}/Yb_{SN} = 0.94 \pm 0.27$, except for samples LG001 and LG005 (Fig. 8I). The rocks show variable La_{SN}/La_{SN}^* (0.86–1.28) and slightly positive Gd_{SN}/Gd_{SN}^* (1.16–1.45) and Y anomalies (Table 1; Fig. 8I). Sample LG001 is markedly silicified ($SiO_2 = 32.21\%$) and has the lowest $\sum$REE value of 0.676 ppm. It shows a zigzag REY pattern similar to those of the skeletal substrates (e.g., corals and clams) from shallow reef framework cavities at Heron Reef, Great Barrier Reef (Webb and Kamber, 2000), which have low content of REE (near or below detection limit). Sample LG005 is a light yellow, recrystallized dolomite-marble with secondary chlorite veinlets (Fig. 7A), just 5 m north to a diabase dyke. It has higher REY content and positive Eu anomaly than other adjacent samples, and the lowest $\delta^{13}C_{carb}$ (3.5‰) and the fourth lowest $\delta^{18}O_{carb}$ (17.4‰) in all 42 samples (Tang et al., 2011).

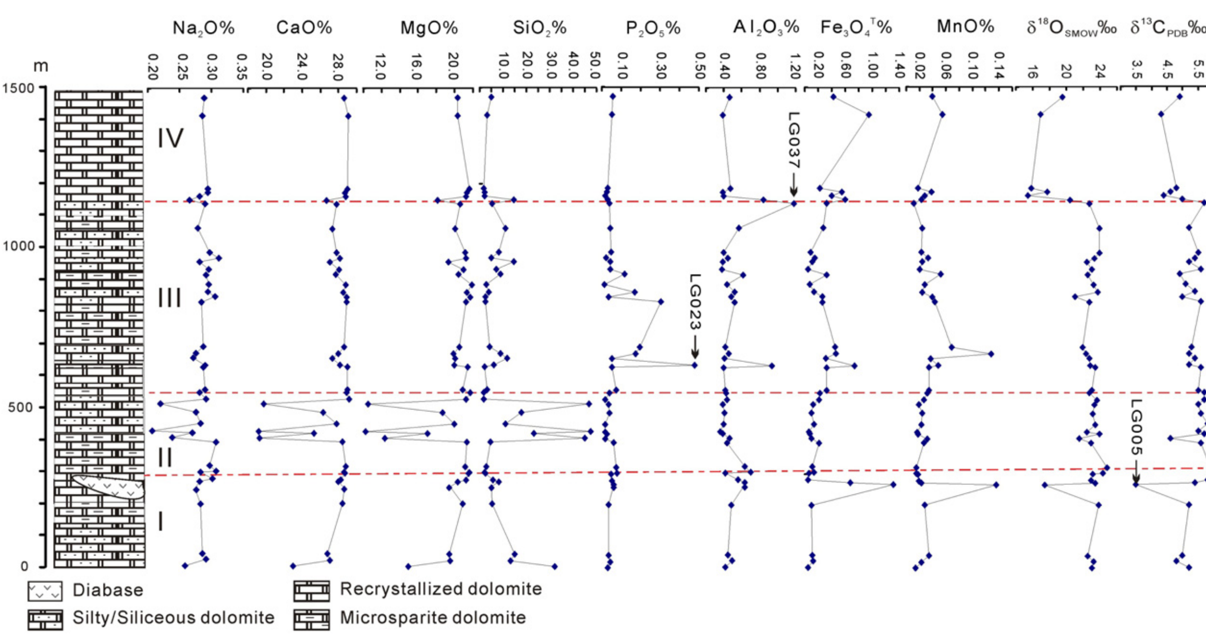

Fig. 5. Petro-chemostratigraphic variations of the Guanmenshan Formation, Liaohe Group.

Please cite this article in press as: Tang, H.-S., et al., REE geochemistry of carbonates from the Guanmenshan Formation, Liaohe Group, NE Sino-Korean Craton: Implications for seawater compositional change during the Great Oxidation Event. Precambrian Res. (2012), doi:10.1016/j.precamres.2012.02.005

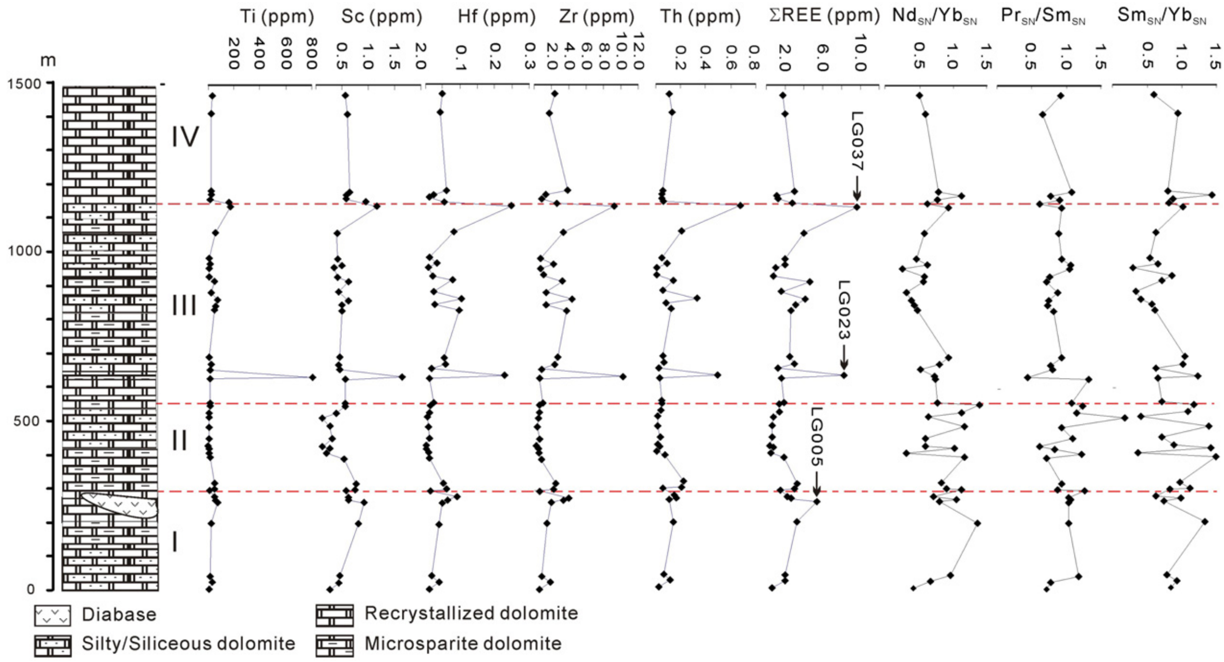

Fig. 6. Trace element chemostratigraphic variation of the Guanmenshan Formation.

Group II includes 12 samples (LG009–LG020) collected from the Guanmenshan Mining area (Figs. 4–6) and characterized by pronounced Eu and LREE enrichments in the smooth, shale-normalized patterns (Fig. 8II). Their Eu_{SN}/Eu_{SN}^* values range from 1.42 to 7.55, average 3.09 ± 1.66, corresponding to Eu_{CN}/Eu_{CN}^* of 0.84–4.45 with an average of 1.89 ± 1.00. They do not show obvious REY fractionation, with $Nd_{SN}/Yb_{SN} = 0.90 \pm 0.32$, $Pr_{SN}/Sm_{SN} = 1.06 \pm 0.33$ and $Sm_{SN}/Yb_{SN} = 0.99 \pm 0.37$, respectively, but have a wide range of $\sum$REE (0.374–3.201 ppm). Six samples of Group II have high (>10%) and variable SiO_2 contents ranging from 10.97 to 47.61%, and low contents of Na_2O, MgO, CaO, Li_2O and MgO/CaO ratio (Table 1, Fig. 5). These six samples also show zigzag-shaped HREE patterns and have low $\sum$REE contents (<0.800 ppm) that decrease with the degree of silicification (Fig. 8II). Under the microscope, hydrothermal quartz aggregates or veinlets and remarkable recrystallization were observed in these samples (Fig. 7B), indicating that they were hydrothermally altered and subjected to silicification.

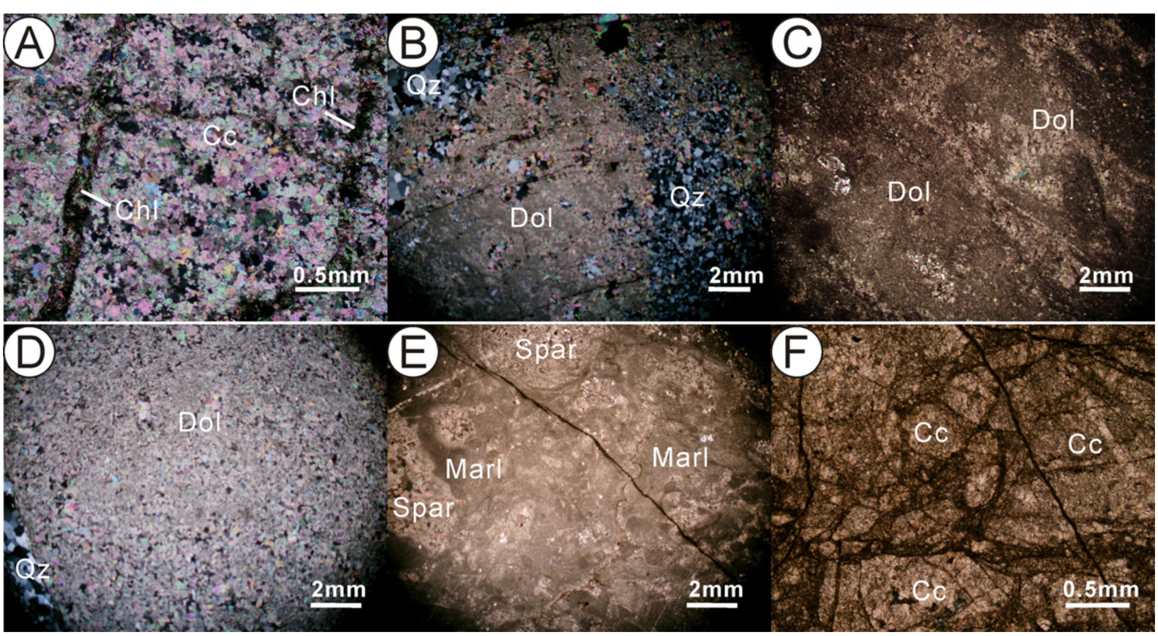

Fig. 7. Photomicrographs of samples from the Guanmenshan Formation, Liaohe Group. (A) Light yellow recrystallized dolomite-marble with secondary chlorite veinlets, collected only 5 m north to a diabase dyke; sample LG005. (B) Intense silicification in dolomite, with quartz clustered into stripped assemblage replacing dolomite, whereas the unreplaced carbonate is generally unrecrystallized and is mostly still dolomicrite. The sample (LG018) was collected from the Guanmenshan mining area. (C) Least altered dolomicrite (sample LG031) without any notable silicification or recrystallization. (D) Local variegated dark gray dolomicrite (sample LG023). (E) Rock dominated by marl/dolomite with limited microspar, and with no obvious secondary altered veins (sample LD037) (F) Gray variegated, severely recrystallized dolomite-marble with veinlets (sample LG041) collected from the Xiaoxigou mining area. Mineral abbreviations: Cc: calcite; Chl: chlorite; Dol: dolomite; Qz: quartz.

Please cite this article in press as: Tang, H.-S., et al., REE geochemistry of carbonates from the Guanmenshan Formation, Liaohe Group, NE Sino-Korean Craton: Implications for seawater compositional change during the Great Oxidation Event. Precambrian Res. (2012), doi:10.1016/j.precamres.2012.02.005

Table 2
The Eu and Ce anomalies and other REY parameters of worldwide chemical sediments of different ages (PAAS-normalized).

Name of strata	Location	Lithology	N	Ga	Y/Ho average (range)	Ce_{SN}/Ce_{SN}^*	Eu_{SN}/Eu_{SN}^*	Pr_{SN}/Sm_{SN}	Nd_{SN}/Yb_{SN}	Sm_{SN}/Yb_{SN}	Data sources
Isua Greenstone Belt	Greenland	BIF	7	3.7–3.8	39.7 ± 5.2 (33.5–47.5)	1.24 ± 0.29	2.17 ± 0.60	0.47 ± 0.19	0.27 ± 0.18	0.41 ± 0.23	Bolhar et al., 2004
Top/Bottom of Sinqeni Fm., Mozaan Gp., Pongola SGp.	S Africa	BIF	8	∼2.9	36.5 ± 2.5 (31.4–39.8)	0.89 ± 0.03	1.82 ± 0.16	0.63 ± 0.15	2.60 ± 0.98	1.22 ± 0.49	Alexander et al., 2008
Middle of Sinqeni Fm., Mozaan Gp., Pongola SGp.	S Africa	BIF	8	∼2.9	46.7 ± 10.8 (35.3–65.5)	0.95 ± 0.09	1.84 ± 0.21	0.80 ± 0.08	1.52 ± 0.35	0.76 ± 0.17	Alexander et al., 2008
Campbellrand	S Africa	Carbonate	5	2.54	76.4 ± 12.6 (55.6–100.2)	0.98 ± 0.04	1.66 ± 0.38	1.05 ± 0.10	0.65 ± 0.29	0.62 ± 0.23	Kamber and Webb, 2001
Kuruman Fm., Transvaal SGp.	S Africa	BIF	13	2.46	45.1 ± 5.0 (40.2 – 57.3)	1.04 ± 0.07	1.75 ± 0.50	0.65 ± 0.08	0.24 ± 0.05	0.32 ± 0.05	Bau and Dulski, 1996
Penge Fm., Transvaal SGp.	S Africa	BIF	6	2.46	52.4 ± 3.0 (48.4–55.2)	1.09 ± 0.08	1.95 ± 0.19	0.79 ± 0.14	0.28 ± 0.05	0.33 ± 0.07	Bau and Dulski, 1996
BIF, Atlantic City	USA	BIF	3	2.72–2.67	32.2 ± 2.0 (31.1–34.5)	1.03 ± 0.05	2.45 ± 0.41	0.68 ± 0.06	0.37 ± 0.04	0.50 ± 0.02	Frei et al., 2008
Nemo BIF, Black Hills	USA	BIF	14	2.89–2.56	43.5 ± 8.2 (34.1–64.6)	1.05 ± 0.09	1.62 ± 0.15	0.69 ± 0.18	0.50 ± 0.27	0.68 ± 0.28	Frei et al., 2008
Benchmark BIF, Black Hills	USA	BIF	6	2.56–2.48	35.6 ± 9.2 (26.7–46.3)	0.95 ± 0.18	1.37 ± 0.21	0.69 ± 0.15	0.76 ± 0.33	1.02 ± 0.30	Frei et al., 2008
Estes conglomerate, Black Hills	USA	BIF	14	2.1–2.02	37.0 ± 8.5 (25.5–52.5)	1.16 ± 0.18	1.34 ± 0.31	0.62 ± 0.13	0.72 ± 0.32	1.09 ± 0.46	Frei et al., 2008
Beizi Gp. Greenstones, NCC	Henan, China	Sediments	5	3.0–2.55		0.81 ± 0.19	1.99 ± 0.35	1.17 ± 0.25	2.26 ± 1.44	2.23 ± 1.56	Chen and Zhao, 1997
Dangzehe Gp. Greenstones, NCC	Henan, China	Chemical/ clastic sediments	6	2.55–2.3		0.73 ± 0.14	2.36 ± 1.70	1.20 ± 0.19	1.68 ± 0.86	1.76 ± 0.96	Chen and Zhao, 1997
Shuidigou Gp. khondalite series, NCC	Henan, China	Chemical/ clastic sediments	4	∼2.3		0.90 ± 0.23	1.45 ± 0.13	0.86 ± 0.21	0.91 ± 0.24	1.11 ± 0.17	Chen and Zhao, 1997
Metamorphic sediments, NCC	Henan, China	Chemical/ clastic sediments	16	2.30–2.15		0.67 ± 0.48	0.92 ± 0.22	1.00 ± 0.38	1.52 ± 0.91	1.63 ± 0.81	Chen and Zhao, 1997
Guanmenshan Fm., Liaohe Gp., NCC	Liaoning, China	Dolomicrite	15	2.3–1.85	44.1 ± 5.7 (34.5–56.6)	0.93 ± 0.09	1.93 ± 0.45	0.90 ± 0.17	0.56 ± 0.19	0.65 ± 0.27	This study
Canning Basin	W Australia	Reefal carbonates microbialites	11	0.365–0.36	45.0 ± 1.8 (42.4–47.7)	0.73 ± 0.04	1.02 ± 0.02	0.70 ± 0.03	0.43 ± 0.02	0.58 ± 0.03	Nothdurft et al., 2004
Great Barrier Reef, Heron Island	E Australia	Holocene reefal microbialites	52	Morden	57.2 ± 2.7 (50.0–61.4)	0.81 ± 0.05	1.21 ± 0.08	0.60 ± 0.03	0.24 ± 0.03	0.35 ± 0.05	Webb and Kamber, 2000

Please cite this article in press as: Tang, H.-S., et al., REE geochemistry of carbonates from the Guanmenshan Formation, Liaohe Group, NE Sino-Korean Craton: Implications for seawater compositional change during the Great Oxidation Event. Precambrian Res. (2012), doi:10.1016/j.precamres.2012.02.005

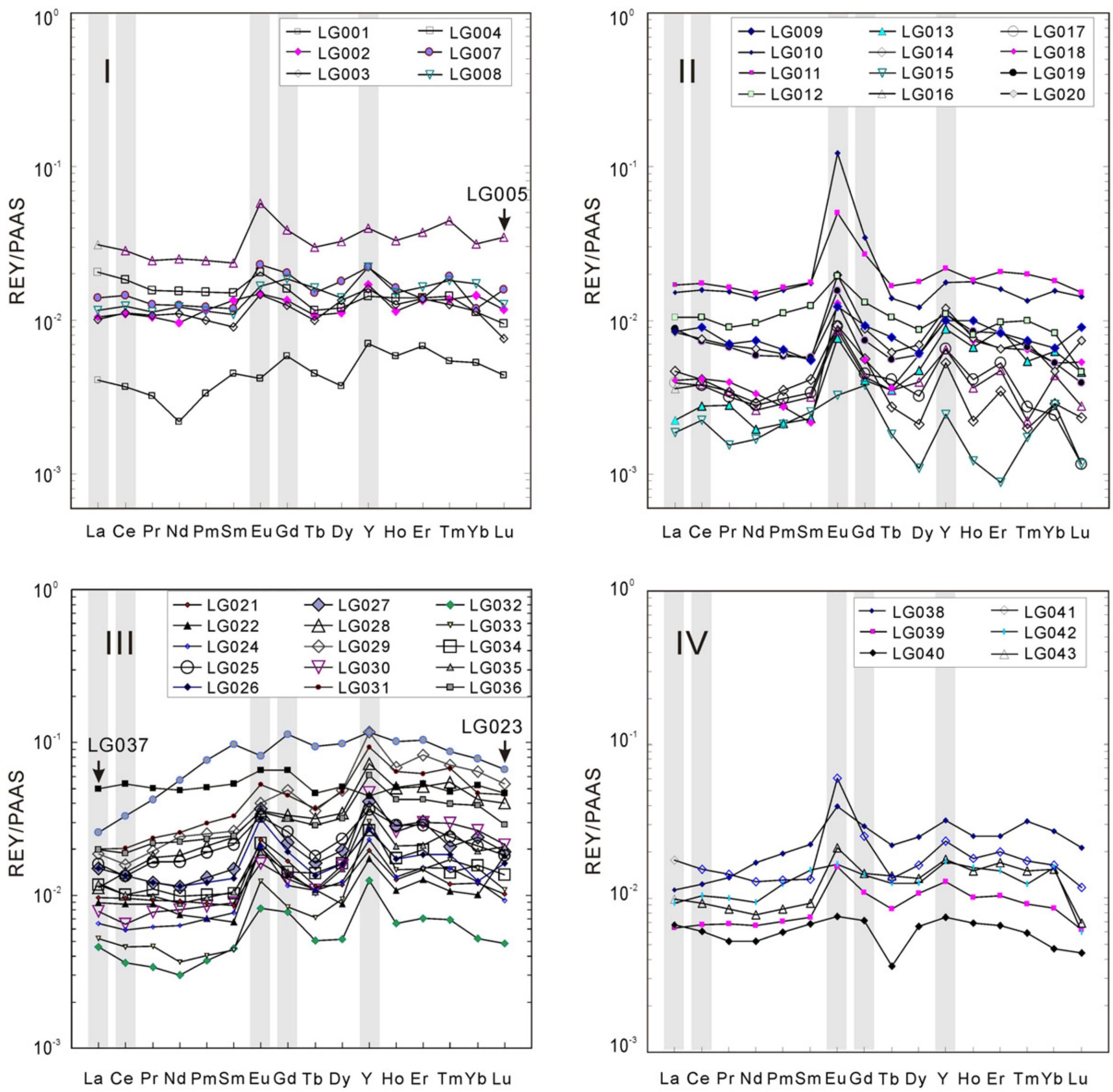

Fig. 8. The PAAS normalized REY patterns for samples from the Guanmenshan Formation. See text for further explanation on classification of the REY groups.

Group III includes dolomicrite (Fig. 7C) samples of LG021–LG037 located in the middle of the stratigraphic column and represents >600 m thick strata (Figs. 4–6). Except for samples LG023 and LG037, all the others show $\sum$REE contents ranging from 0.739 to 4.597 ppm with average of 2.414 ± 1.181 ppm (n = 15), and seawater-like REY patterns (Fig. 8III; normalized to PAAS) characterized by: (1) strong and uniform LREE depletion, with Nd_{SN}/Yb_{SN}, Pr_{SN}/Sm_{SN} and Sm_{SN}/Yb_{SN} ranging 0.24–0.92 (average 0.56 ± 0.19), 0.71–1.32 (average 0.90 ± 0.17) and 0.29–1.04 (average 0.65 ± 0.21), respectively; the ratios of the modern shallow seawater are 0.21–0.27, 0.52–0.63 and 0.26–0.38, respectively (Alibo and Nozaki, 1999); (2) superchondritic Y/Ho ratios, ranging from 34.5 to 56.6 with average of 44.1 ± 5.7 (Table 2), higher than those of the chondrite (24.7) and the upper continental crust (27.5) (Taylor and McLennan, 1985); (3) notable positive Y anomalies (Fig. 8III); (4) slightly positive La-anomalies ranging 0.69–1.90 with average of 1.04 ± 0.27 (Table 1). These features are remarkably consistent with those of the 2.10–2.02 Ga South Dakota BIF (Frei et al., 2008) and most Archean samples (Fig. 9A), and are obviously lower than those of the modern seawater (3.47–4.24; Alibo and Nozaki, 1999); and (5) consistently positive Gd-anomalies (Gd_{SN}/Gd_{SN}^* = 1.05–2.32, with average of 1.64 ± 0.40), which are similar to most ancient marine sediments (Fig. 9B) and slightly higher than those of the modern seawater (Gd_{SN}/Gd_{SN}^* = 1.08–1.19; Alibo and Nozaki, 1999). In addition, the rocks also show weak negative Ce-anomalies (Ce_{SN}/Ce_{SN}^* = 0.93 ± 0.09). Sample LG023 (Figs. 5, 6, 7D, 8III) is characterized by a roof-shaped REY pattern (Pr_{SN}/Sm_{SN} = 0.43, Sm_{SN}/Yb_{SN} = 1.23) with the highest P_2O_5 (0.478%) and Zr (10.273 ppm) contents among all the samples, and high $\sum$REE (8.282 ppm), Al_2O_3 (0.93%), Th (0.496 ppm) and Hf (0.225 ppm) abundances, but relatively low Y/Ho ratio (31.2). Its La_{SN}/La_{SN}^*, Ce_{SN}/Ce_{SN}^* and Gd_{SN}/Gd_{SN}^* values are 1.95, 1.20 and 1.26 (Table 1), respectively, showing positive anomalies (Fig. 8III), but Eu_{SN}/Eu_{SN}^* (=0.85 or Eu_{CN}/Eu_{CN}^* = 0.52) is the lowest. Sample LG037 (Figs. 5, 6, 7E, 8II I) has a flat REY pattern and the highest $\sum$REE (9.616 ppm), Al_2O_3 (1.18%), Th (0.678 ppm) and Hf (0.248 ppm) contents. The Zr content of this sample is relatively high (9.282 ppm), but the Y/Ho ratio is the lowest (24.0). It shows no clear La- and Ce-anomalies, with La_{SN}/La_{SN}^* = 0.93 and Ce_{SN}/Ce_{SN}^* = 1.03, respectively.

Group IV includes samples LG038–LG043 collected from the uppermost portion of the stratigraphic column, and represents ca. 300 m thick strata (Figs. 4–6). These samples consist of gray variegated, severely recrystallized and veinlet-filled dolomite-marbles

Please cite this article in press as: Tang, H.-S., et al., REE geochemistry of carbonates from the Guanmenshan Formation, Liaohe Group, NE Sino-Korean Craton: Implications for seawater compositional change during the Great Oxidation Event. Precambrian Res. (2012), doi:10.1016/j.precamres.2012.02.005

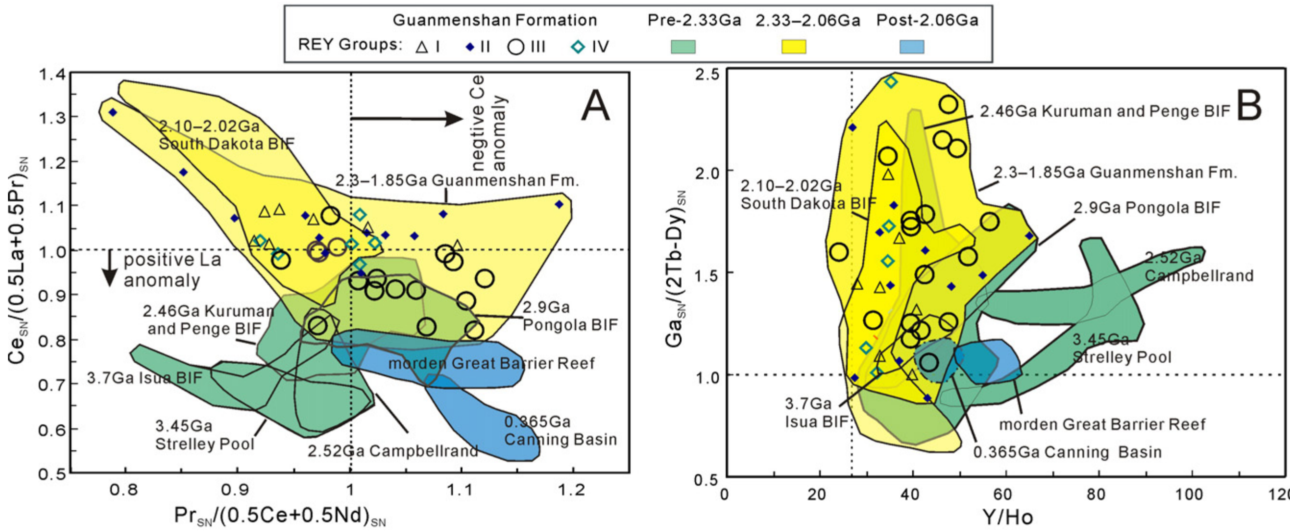

Fig. 9. (A) $[Ce/(0.5La+0.5Pr)]_{SN}$ vs. $[Pr/(1/2Ce+1/2Nd)]_{SN}$, used to show La and Ce anomalies in seawater-derived sediments (base map after Bau and Dulski, 1996; Bolhar et al., 2004); 2.3–1.85 Ga Guanmenshan carbonates are distinct from other bona fide Archean and post-Archean seawater precipitates, (B) binary plot of Y/Ho vs. $[Ga/(2Tb-Dy)]_{SN}$, comparing Guanmenshan Formation carbonates with bona fide seawater precipitates from the literature. Data sources are from Table 2, with the addition of data for the average Strelley Pool stromatolite (Van Kranendonk et al., 2003). See Fig. 8 for sample REY groups.

(Fig. 7F), and were collected from a fracture zone south of the Xiaoxigou Pb–Zn Mine (Fig. 4). These rocks have relatively high contents of MnO and Fe_2O_3 (Fig. 5) and variable REY patterns (Fig. 8IV), but most (LG039, LG041 and LG043) preserve similar REE abundances and REY patterns as to those of Group II.

5. Discussion

5.1. Constraints on REY in the Guanmenshan Formation

To utilize REY as a tool for tracing the features of the input sources, sedimentary processes as well as environment changes, the geochemical behavior of REY during deposition and post-depositional geological processes must be properly understood. The sediment compositions are commonly controlled by source compositions, diagenetic processes and sedimentary environments (Chen, 1996; Chen and Zhao, 1997; Nozaki et al., 1997). Compositional features of detrital sediments are mainly controlled by the source rock properties and the weathering–transportation–deposition processes. The element geochemistry of modern shales mainly reflects the weathering degree of the source rocks (Nesbitt et al., 1990), because the impact of transportation, deposition, diagenesis and subsequent metamorphism on REY is very weak (Bhatia, 1983; Bhatia and Crook, 1986; Taylor and McLennan, 1985). Consequently, the geochemistry of elements (e.g., REY, Th, Sc, Hf, Co and several major elements) in clastic rocks is extensively utilized to trace input sources and tectonic settings of basins (Bhatia, 1983; Bhatia and Crook, 1986; Girty et al., 1994). However, the geochemistry of marine chemical sediments (e.g., carbonates) is mostly controlled by depositional environment (Chen, 1996; Chen and Zhao, 1997; Nothdurft et al., 2004; Bolhar and Van Kranendonk, 2007). The REY in the Guanmenshan Formation might be affected by (i) the geochemical behavior of REY in seawater, (ii) syndepositional contamination of various inputs, and (iii) post-depositional diagenesis and metamorphism.

5.1.1. Fundamental REY geochemistry in seawater and chemical sediments

Many studies in the past (e.g., Webb and Kamber, 2000; Kamber and Webb, 2001; Bolhar et al., 2004; Nothdurft et al., 2004; Bolhar and Van Kranendonk, 2007) have summarized modern seawater or chemical sediment REY patterns (normalized to a shale standard) and show the following salient features: (1) positive La_{SN} anomaly, which reflects enhanced stability of La in solution and may be related to the absence of inner 4f electrons (De Baar et al., 1985; Bolhar et al., 2004); (2) negative Ce_{SN} anomaly caused by the oxidation of Ce(III) into less soluble Ce(IV) in modern oxic ocean system and then scavenged by suspended particles that settle through the water column (Sholkovitz et al., 1994; Bau and Dulski, 1996). A conspicuous positive Ce_{SN} anomaly is observed in alkaline waters (e.g., the Lake Van, Turkey, pH 9.6; Möller and Bau, 1993), which is probably due to the stabilization of polycarbonato-Ce(IV) complexes in solution. Most Archean chemical sediments lack obvious Ce_{SN} anomalies (positive or negative), suggesting that the fO_2 was low in the surficial environment at that time (Bau and Dulski, 1996; Frei et al., 2008; Alexander et al., 2008); (3) positive Gd_{SN} anomaly due to lower surface complexation stability, which weakens the particle stability and subsequent scavenging, and makes Gd enriched in solution relative to its neighbors in the REE series (De Baar et al., 1985; Lee and Byrne, 1992); (4) high Y/Ho ratio (44–74; Byrne and Lee, 1993; Bau, 1996; Nozaki et al., 1997) that results from both the preferential sorption of Ho relative to Y on the scavenging Fe–Mn particles (Bau, 1999) and the fractionation during crustal weathering and transportation because of easier surface complexation behaviour or higher solubility of Y relative to Ho-phosphates (Nozaki et al., 1997). The Y/Ho ratios of continental clasts and volcanic debris are constant at ~28 (Bau, 1996) and similar to those of the chondrite (24.7; Taylor and McLennan, 1985); and (5) LREE and MREE depletions relative to HREE ($Sm_{SN}/Yb_{SN} < 1$; $Nd_{SN}/Yb_{SN} < 1$); due to the lanthanide contraction effect, as particles settle through the water column, LREE and MREE are being preferentially adsorbed while the HREE are preferentially retained in solution (Chen and Zhao, 1997). The preference to form carbonate complexes increases from La to Lu, thereby enhancing the HREE enrichment (Tu et al., 1985; Chen and Fu, 1991; Lee and Byrne, 1992; Sholkovitz et al., 1994).

The REY concentration in modern seawater is controlled primarily by the "scavenging" of certain particles (Erel and Stolper, 1993) that absorb and precipitate the REY, and result in the extremely low REY abundances in seawater. On the basis of the intimate association between Fe-rich colloids and REY, Derry and Jacobsen (1990) suggested that Fe–oxyhydroxide particles dominated REY

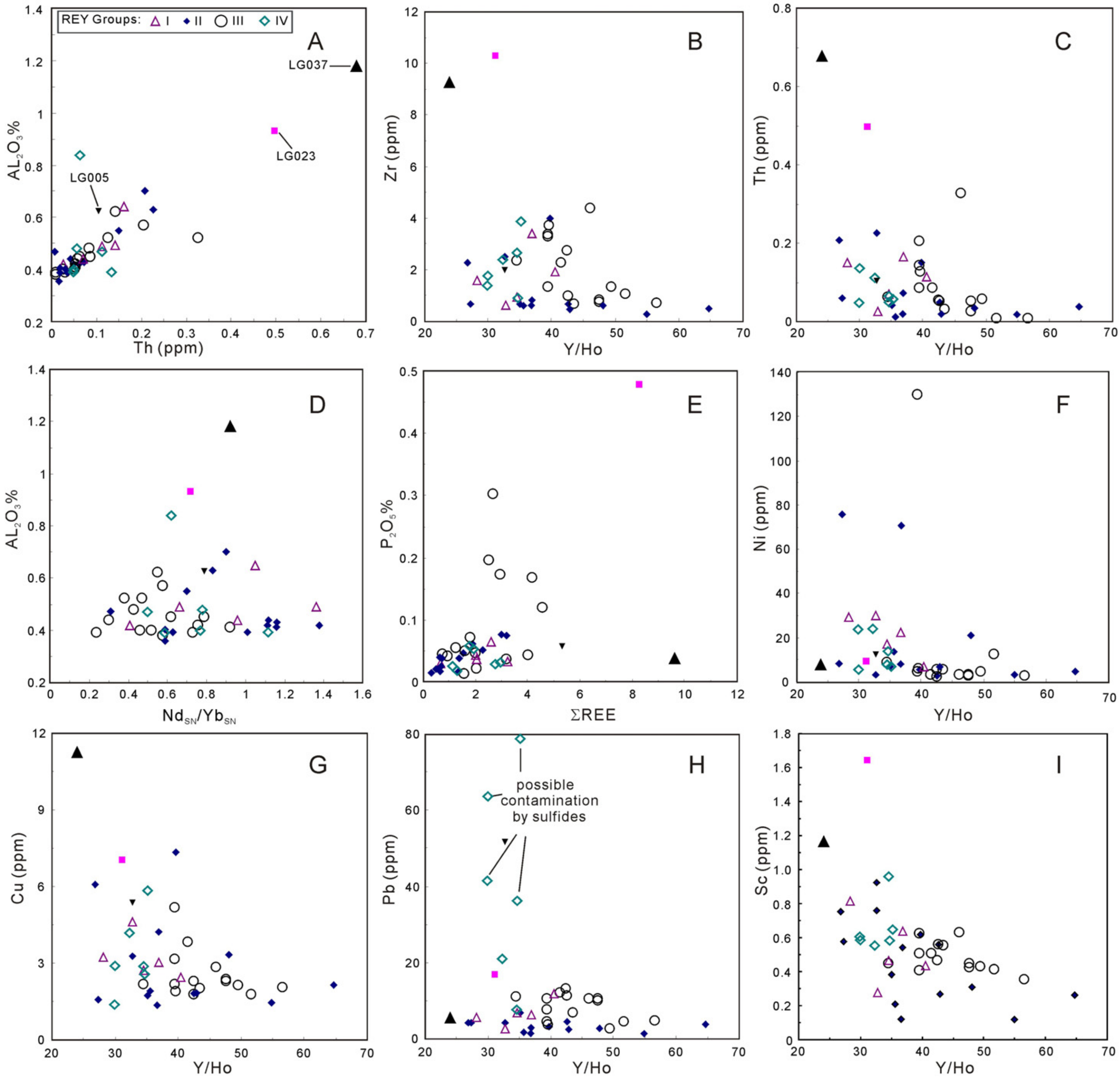

Fig. 10. Correlation of REY with other elements The poor correlations of Th with Al_2O_3 content (A), and of Y/Ho with Zr and Th concentrations (B and C) as well as the low contents of Zr and Th suggest that terrestrial debris had not contaminated the chemical sedimentation of the Guanmenshan Formation. Plot of Al content vs. LREE depletion (Nd_{SN}/Yb_{SN}) in the Guanmenshan Formation samples show poor overall correlation and suggest that LREE depletion is affected by parameters other than shale contamination (D). The P_2O_5 contents are very low and show no correlation with $\sum$REE (E), suggesting that phosphate input did not change REE patterns of the samples. Fe-oxide contamination can be ruled out due to poor correlations of Y/Ho values with Cu and Ni contents (F and G), and low concentrations of Ni and Cu. Pb and Sc concentrations are very low and are not correlated with Y/Ho (H and I), suggesting that sulfide contamination did not change REE patterns of the samples.

scavenging during the formation of ancient metalliferous sediments. Experiments demonstrated that the adsorption/desorption is notably faster than the particles residence time in an oxic water column and the particle-surface/solution REY exchange equilibrium occurs within minutes (Bau, 1999). Bau et al. (1998) pointed out that very similar fractionation is observed between modern marine hydrogenetic ferromanganese crusts and terrestrial spring-water precipitates. The striking difference between these precipitates (Y/Ho = 12.9–17.6; n = 2) and fluids (Y/Ho = 52.3–59.2; n = 7) displays negative Y anomalies in sediments. This Y–Ho fractionation is due to the preferential adsorption of Ho over Y on Fe–oxyhydroxides particles (Bau et al., 1996, 1998; Bau, 1999). The significantly higher Y/Ho ratios in BIFs of different ages (Table 2) than those of the Fe–oxyhydroxide particles (Bau et al., 1996) strongly suggests that the scavenged REY could not be at or near exchange equilibria with ambient seawater (Bau and Dulski, 1996).

5.1.2. Contamination

The REY features of the chemical sediments might be masked due to contamination. Such contamination must be ruled out in order to interpret REY data properly. Possibly significant sources

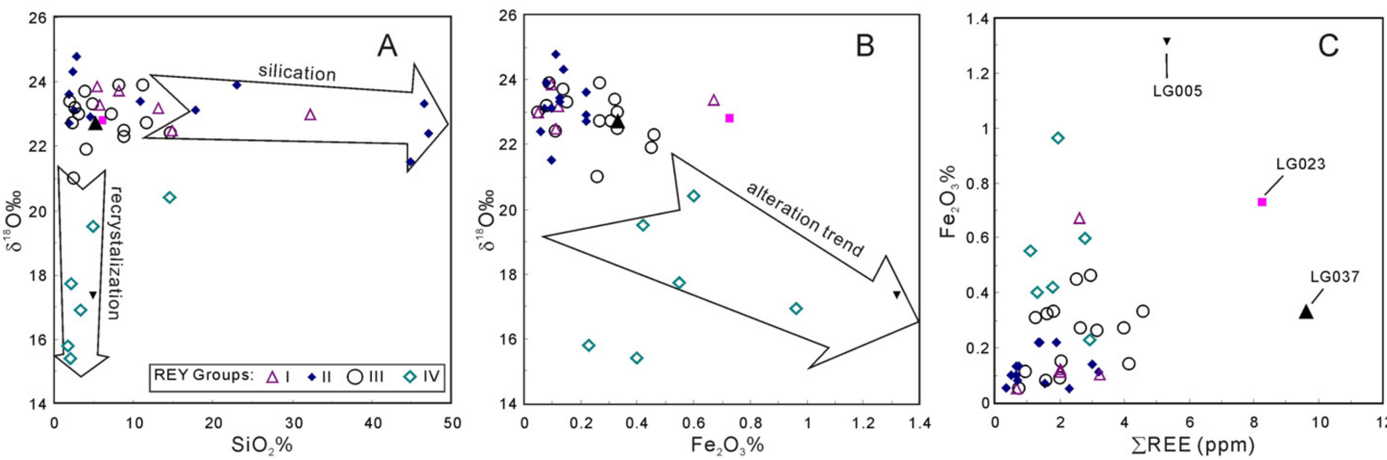

Fig. 11. Geochemical variation of the Guanmenshan Formation during diagenesis. (A) Plot of $\delta^{18}O_{carb}$ vs. SiO_2 content, showing contrasting silication and recrystalization trends. (B) Plot of $Fe_2O_3^T$ content vs. $\delta^{18}O_{carb}$, showing significant variations at the Xiaoxigou mining area. (C) Correlations of $Fe_2O_3^T$ contents with ∑REE, suggesting that the REE patterns of the Guanmenshan Formation were affected by parameters other than diagenesis.

of contamination include terrestrial detritus, Fe- or/and Mn-oxide, sulfide and phosphate.

Terrestrial particulate matter (e.g., shale) is a major input source for marine REY, but has high REY concentration with distinctly non-seawater-like pattern (Goldstein and Jacobsen, 1988; Elderfield et al., 1990). A small quantity (e.g., 1–2%) of shale would sharply reduce the La_{SN} and Ce_{SN} anomalies and abruptly decrease the degree of LREE depletion (Nothdurft et al., 2004). Notable shale contamination can thoroughly change the seawater-like REY patterns of carbonate into shale-like REY patterns with pronounced high ∑REE values (Nothdurft et al., 2004); and the abundances of lithophile elements (e.g., Al, Ti, Th, Hf, Zr) intimately related to terrigenous detritus will greatly increase and show a strong positive correlation with increased Al concentration (Bolhar et al., 2004; Bolhar and Van Kranendonk, 2007; Alexander et al., 2008). For instance, Bau and Dulski (1996) noticed that the REY patterns of shale contaminated samples ($Al_2O_3 > 0.5\%$ and/or Sc > 0.43 ppm) from the 2.46 Ga Penge BIFs, Transvaal Supergroup, South Africa altered significantly, while the pure chemical sedimentary BIFs (e.g., Sc < 0.43 ppm, Th < 0.1 ppm, and Hf < 0.1 ppm) retained seawater-like REY patterns. The terrestrial material (i.e. felsic and basaltic crust) and chondrite have constant Y/Ho ratios of 26–28 (Webb and Kamber, 2000; Bolhar et al., 2004), and therefore, a small admixture of any contaminant will reduce the Y/Ho ratios of seawater or marine chemical sediments (Bau et al., 1996; Webb and Kamber, 2000).

The siderophile elements (e.g., Ni and Sc) are preferentially enriched in the sediments contaminated with Fe- and/or Mn-oxides, though they incorporate REE disproportionately and unpredictably (Bau et al., 1996), and have negative correlation with Y/Ho ratios or Ce_{SN}/Ce_{SN}^* (Bolhar and Van Kranendonk, 2007). The chalcophile elements (e.g., Pb, Zn and Cu) in the sediments can be enriched by sulfide contamination and have negative correlations with Y/Ho ratios (Nothdurft et al., 2004; Bolhar and Van Kranendonk, 2007). The phosphates have a high affinity for REY in diagenetic fluids and in some cases show non-uniform incorporation across the REE mass range (Byrne et al., 1996; Shields and Stille, 2001).

In summary, a small admixture of any contaminants can notably reduce the Y/Ho ratios of marine chemical sediments and enhance co-variations between Y/Ho, Ce_{SN}/Ce_{SN}^* (in modern seawater proxies), Pr_{SN}/Yb_{SN}, La_{SN}/La_{SN}^* and abundances of identifying elements of terrestrial crust, such as Al, Ti, Zr, Hf, Th and Sc (Bolhar et al., 2004; Bolhar and Van Kranendonk, 2007).

Shale has not been observed in the Guanmenshan Formation in the Guanmenshan area. Chlorite and other secondary minerals are not also observed in petrographic study. Except for the fractured and recrystallized dolomite-marbles of the Guanmenshan Formation (Fig. 7F), the alteration and weathering of the samples are very weak. The concentrations of Zr (0.278–4.360 ppm), Th (0.007–0.207 ppm), Hf (0.002–0.103 ppm) and Sc (0.115–0.963 ppm) of the samples (except LG023 and LG037, as discussed below) are generally low (Table 1). The Al_2O_3 concentrations are 0.36–0.87%, consistent with those of the Paleoproterozoic dolostone ($Al_2O_3 = 0.70 \pm 0.49\%$; Veizer et al., 1992). The poor correlations of Th with Al_2O_3 content (Fig. 10A), and of Y/Ho with Zr and Th concentrations (Fig. 10B and C), as well as the low contents of Zr and Th suggest that terrestrial debris did not contaminate the chemical sedimentation of the Guanmenshan Formation. Plots of Al contents vs. Nd_{SN}/Yb_{SN} ratios in the Guanmenshan Formation show poor correlation and suggest that the LREE depletion is unlikely affected by detrital contamination (Fig. 10D). As mentioned above, sample LG023 has a convex REY pattern that is usually observed in phosphates (Shields and Stille, 2001), suggesting that the sedimentary environment was oxic and prosperous with biological activity. This is supported by the far higher P_2O_5 content than the other samples and high ∑REE content in sample LG023 (Figs. 5, 6, 10E). The P_2O_5 contents in other samples are very low and do not correlate with ∑REE (Fig. 10E), and do not suggest any phosphate impact on REY patterns. Fe-oxide contamination to the sedimentation of the Guanmenshan Formation can be ruled out due to low contents of Ni and Cu and their poor correlations with the Y/Ho ratios (Fig. 10F and G). Moreover, Pb and Sc contents are also very low and are not correlated with Y/Ho (Fig. 10H and I), excluding the possibility of sulfide contamination. On the other hand, fractured and recrystallized dolomite-marbles at the Xiaoxigou Pb–Zn mine area, have relatively high Pb contents, likely contaminated by sulfides (Fig. 10H).

Sample LG037 is dominated by marl/dolomite with limited microspar (Fig. 7E), and has flat shale-normalized REY pattern (Fig. 8III). It is obviously richer in terrigenous detritus-intimate incompatible elements (e.g., Al, Ti, Th, Hf, Zr, Sc) as compared to the other samples (Table 1, Fig. 10), and is also richer than the recognized shale-contaminated samples ($Al_2O_3 > 0.5\%$ and/or Sc > 0.43 ppm) from the 2.46 Ga Penge BIFs, Transvaal Supergroup,

Please cite this article in press as: Tang, H.-S., et al., REE geochemistry of carbonates from the Guanmenshan Formation, Liaohe Group, NE Sino-Korean Craton: Implications for seawater compositional change during the Great Oxidation Event. Precambrian Res. (2012), doi:10.1016/j.precamres.2012.02.005

South Africa (Bau and Dulski, 1996). These features show that the strata represented by sample LG037 were contaminated by shale or terrigenous detritus.

5.1.3. Impact from post-depositional processes

Diagenesis, metamorphism and fluid flow are three commonly considered geological processes which affect the REY geochemical signatures of the chemical sediments. Based on the study of BIFs in Hamersley (Western Australia), Broomstock (Zimbabwe), and Kuruman and Penge (South Africa), Bau (1993) showed that REY could not be mobilized during diagenesis. Banner and Hanson (1990) studied the dolomites of the Mississippian Burlington-Keokuk Formation and showed that during diagenetic water–rock interaction the C and Nd isotope ratios and REE contents did not show notable change when the fluid/rock ratio (on a weight basis) is below 1000, although the $^{87}Sr/^{86}Sr$ ratios increased, and the $\delta^{18}O$ values and Sr contents decreased. In general, hydrothermal processes reduced Sr concentration and increased Mn, Fe and Rb concentrations in carbonate rocks (Brand and Veizer, 1980; Veizer, 1983; Veizer et al., 1999; Jacobsen and Kaufman, 1999; Melezhik et al., 2001a,b, 2005, 2006, 2008; Bekker et al., 2001, 2003a,b, 2005).

Metamorphism has little effect on REY mobility; however, intense hydrothermal alteration associated with metamorphic processes could result in LREE depletions and negative Eu anomalies in carbonate rocks (Bau, 1993). For instance, the high-grade metamorphosed BIFs in the 3.7 Ga Isua Supergroup (Greenland) do not show Eu- or LREE-depletion, and similar detritus-free BIFs in other areas display similar REY patterns regardless of the metamorphic grade (Bau, 1991, 1993). Accordingly, the REY geochemical characteristics of very low-grade metamorphosed Guanmenshan Formation cannot be related to metamorphism, but indicates local hydrothermal alteration of the rocks.

In Fig. 11A, the fractured and recrystallized dolomite-marble samples from the Xiaoxigou Mine (Fig. 7F) cluster in a recrystallization trend. They have low SiO_2 contents (<5%), lower $\delta^{18}O$ values than the other samples of the Guanmenshan Formation, and variable REY patterns (Fig. 8IV), suggesting the effects of hydrothermal alteration. The samples from the Lidigou area (Fig. 4) mainly cluster in a silicification trend (Fig. 11A), with high $\delta^{18}O$ ratios, which can be interpreted as the "seal" protection of the carbonate O-isotope systems because quartz formed from diagenetic silication generally has high $\delta^{18}O$ (Bau et al., 1999).

The most intensely silicified samples have the lowest REY concentrations, accompanied by the decrease in other main components (Table 1; Figs. 5 and 6), but they still have REY patterns similar to the other dolostones in adjacent strata (Fig. 8II). The $Fe_2O_3^T$ contents in the carbonates of the Guanmenshan Formation are not higher than 1.32% (Table 1), and slightly lower than the worldwide Paleoproterozoic carbonates ($Fe_2O_3^T = 1.61 \pm 0.44\%$; Veizer et al., 1992). However, they show increase with silicification (Fig. 11B), particularly as displayed by sample LG005 which was affected by the diabase dyke intrusion (Figs. 4 and 7A). The MnO contents show similar increasing trend (Table 1), companied with the $\delta^{18}O_{Carb}$ decrease (Fig. 11B) possibly caused by hydrothermal alteration (Tang et al., 2009, 2011). The poor correlation of $Fe_2O_3^T$ contents with $\sum$REE (Fig. 11C) suggests that the REY patterns of the Guanmenshan Formation are affected by factors other than diagenesis.

Fifteen samples from the Guanmenshan and Xiaoxigou mining areas (Fig. 8II and IV) have consistent REY patterns, characterized by pronounced Eu_{SN} enrichments in shale-normalized trace element patterns, with $Eu_{CN}/Eu_{CN}^* = 0.83–4.45$ and average of 1.56 ± 0.95. In modern marine environments, the pronounced positive Eu anomalies are only observed in high-temperature (>250 °C) hydrothermal systems typically developed at mid-ocean ridges and back-arc spreading centers, where alteration of seafloor basalts or mafic rocks contribute both REY, together with Fe^{2+} and Mn^{2+} to the hydrothermal systems (Bau and Dulski, 1996, 1999). High-temperature (>250 °C) hydrothermal systems have higher $(Eu/Eu^*)_{CN}$ (>1) and $(Sm/Yb)_{CN}$ ratios than the low-temperature (<250 °C) ones (Pichler et al., 1999; Wheat et al., 2002), but both have positive ε_{Nd} values (Bau and Möller, 1993).

The homogenization temperatures of fluid inclusions in dolomite at the Guanmenshan and Xiaoxigou mining areas range from 141 to 341 °C, and mainly fall in the region of 170–260 °C,

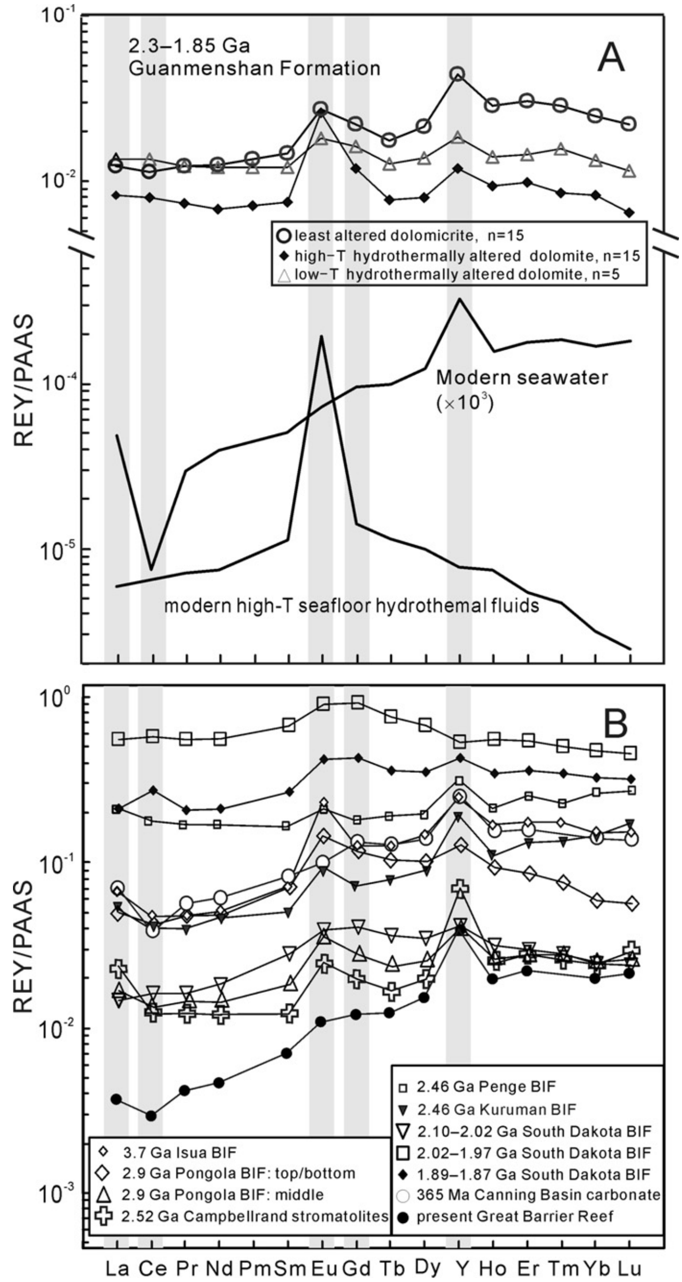

Fig. 12. PAAS-normalized REY diagrams for seawater proxies and Guanmenshan Fm. (A) Samples of the Guanmenshan, modern seawater (depth < 500 m, Pacific seawater, data cited from Alibo and Nozaki, 1999) and high-T (>350 °C) marine hydrothermal fluids (Bau and Dulski, 1999); (B) averages of Archaean to Paleoproterozoic carbonates and banded iron formations (BIF), data sources: 3.7 Ga Isua BIF (Bolhar et al., 2004); 2.9 Ga Pongola BIF (Alexander et al., 2008); 2.52 Ga Campbellrand stromatolites (Kamber and Webb, 2001); 2.46 Ga Kuruman and Penge BIFs (Bau and Dulski, 1996); 2.10–1.87 Ga South Dakota BIF (Frei et al., 2008). Devonian reef carbonates (375–360 Ma; Nothdurft et al., 2004); and recent microbialites from Great Barrier Reef (Webb and Kamber, 2000).

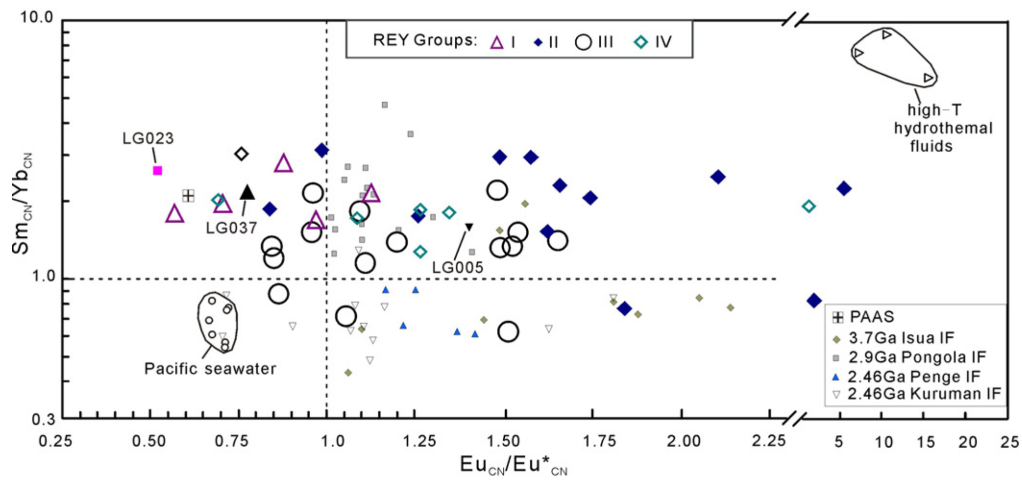

Fig. 13. Plot of $Sm_{CN}/Yb)_{CN}$ vs. Eu_{CN}/Eu_{CN}^* for the Guanmenshan Formation. See Fig. 12 caption for data sources. All samples have significantly lower Sm_{CN}/Yb_{CN} and Eu_{CN}/Eu_{CN}^* than high-T hydrothermal fluids.

and the homogenization temperatures of fluid inclusions in quartz show a range of 87–320 °C (Rui et al., 1991). These results clearly show that the carbonate strata at the Guanmenshan and Xiaoxigou mining areas strongly interacted with high-temperature hydrothermal fluids. Therefore, the REY patterns of those 15 samples mentioned above, similar to modern seafloor high-temperature hydrothermal systems, cannot record the seawater REY features, but suggest that the ore-hosting strata might have been altered by high-temperature hydrothermal fluids, or contaminated by syn-depositional seafloor hydrothermal sedimentation. In addition, the REY patterns of silicified dolomites shown in Fig. 8I, possibly record the REY signatures of locally low-temperature hydrothermal activity (Wheat et al., 2002).

5.2. Paleoproterozoic seawater composition

As discussed above, part of the samples of the Guanmenshan Formation dolostones record the REY compositions and changes in Paleoproterozoic seawater. The dolomicrite rocks from the middle of the stratigraphic column of the Guanmenshan Formation have the most consistent seawater-like shale-normalized REY patterns, with LREE depletions and positive La, Gd, and Y anomalies (Fig. 8III), and similar to those of the worldwide chemical sediments of different ages (Fig. 12), suggesting that these samples preserve robust REY geochemical signatures of contemporaneous seawater, and thereby can be used to trace the nature of the 2.33–2.06 Ga hydrosphere–atmosphere system.

In general, the >2.3 Ga chemical sediments are enriched in Eu, with $Eu_{CN}/Eu_{CN}^* > 1$ (Fig. 13) which is a common REY feature of Archean sediments (Derry and Jacobsen, 1990), and suggests that the seafloor high-temperature hydrothermal fluids were quite active in Archean, and/or, the fO_2 was low in Archean atmosphere–hydrosphere system (Chen and Fu, 1991; Chen and Zhao, 1997). The REY features of the Guanmenshan Formation dolomicrite are characterized by $Eu_{CN}/Eu_{CN}^* \approx 1$ (or slightly >1) and $Sm_{CN}/Yb_{CN} > 1$, distinctly different from those of the >2.3 Ga chemical sediments (Fig. 13), suggesting that the formation of theses rocks did not occur in >2.3 Ga anoxic environment.

Modeling calculation for two-endmember mixing system shows that the Eu/Sm ratios of the Guanmenshan Formation could be accounted by a 1% contribution of high-T fluids to the modern seawater (Fig. 14A; Bau and Möller, 1993), but the Y/Ho and Sm/Yb ratios must be matched up by a >5% contribution of high-T fluids (Fig. 14B). This discrepancy in mixing ratios (Fig. 14C) shows that the REY signatures of the Guanmenshan Formation cannot be explained by synsedimentary hydrothermal fluid mixing, suggesting that the composition of Paleoproterozoic seawater was different from the modern seawater and its mixing with hydrothermal fluids.

The river water is another possible contributor to REY in the Guanmenshan Formation. The samples from the top and bottom of the 2.9 Ga Pongola BIF-containing sequence have notable higher Sm_{CN}/Yb_{CN} ratios than those from the middle section of the Pongola sequence and other Arhean BIFs (Fig. 13), which is linked to the input of river water during sedimentation of the Pongola BIF (Alexander et al., 2008). Elderfield et al. (1990) reported REY data for five coastal seas (salinity > 20‰), and six estuarine waters (salinity < 10‰) as well as 15 rivers that have Sm_{CN}/Yb_{CN} ratios of 0.7–1.24, 0.63–4.74 and 0.93–4.74, respectively, and deduced that the colloidal particles in river water might be enriched in the MREE (shale-normalized) relative to the light and heavy REY. Studies of the Kalix River in Sweden demonstrated that the Fe- and C-rich colloidal particles (Andersson et al., 2006), are enriched in MREE and HREE, and the Fe-rich organic colloids are generally enriched in MREE (Sholkovitz and Szymczak, 2000; Hannigan and Sholkovitz, 2001). These results can help in understanding the formation of BIFs in the shallowest sea, and can be employed to interpret the slight MREE enrichment in the Guanmenshan dolostone.

In summary, as indicated by the REY in the Guanmenshan Formation, the 2.3–2.06 Ga seawater was unique in composition, compared to Archean and Phanerozoic.

5.3. Paleoproterozoic environment change: the Lomagundi Event

Carbonate and BIF are two important chemical sediments which can be used to trace the nature and evolution of the Earth's hydrosphere–atmosphere system (Chen, 1996; Huston and Logan, 2004; and references therein). The application to BIFs has been well documented (Table 2, Fig. 15; Huston and Logan, 2004; Frei et al., 2008). Precambrian BIFs are generally divided into the Algoma- and Superior-types (Gross, 1983) and mainly formed in Paleoproterozoic when the fO_2 in seawater was high enough to oxidize Fe^{2+} into Fe^{3+} (Fig. 15) to form voluminous BIFs (Huston and Logan, 2004). The pre-2.33 Ga BIFs are mainly Algoma-type (dominated by F_3O_4) associated with greenstone belts (e.g., Zhang et al., 2011); whereas the post-2.06 Ga BIFs are dominated by Superior-type (dominated by Fe_2O_3) associated with the stable sedimentary basins and cratonic margins. The size of Superior-type BIF Fe

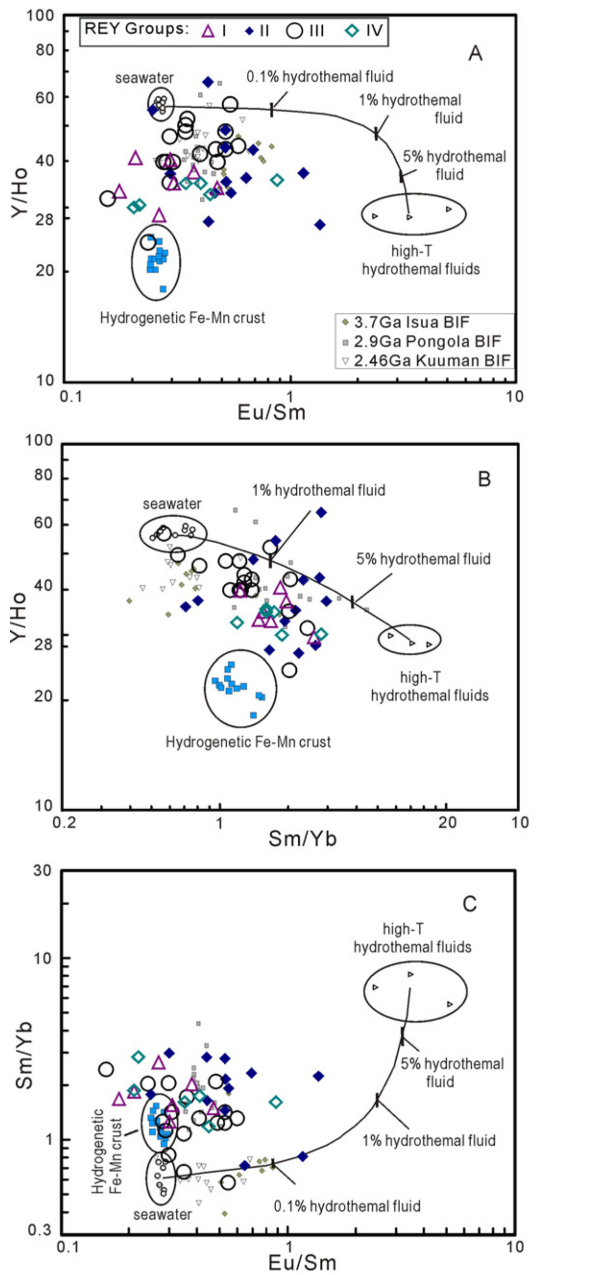

Fig. 14. Plots for Eu/Sm, Sm/Yb and Y/Ho and conservative two-component mixing lines. (A) Y/Ho vs. Eu/Sm; (B) Y/Ho vs. Sm/Yb; (C) Sm/Yb as a function of Eu/Sm. Data sources: hydrogenetic marine ferromanganese crust (Bau et al., 1996), other data sets are presented in Fig. 12.

deposits generally range 10^5–10^8 Mt, far larger than the Algoma-type of 10^3–10^7 Mt (Huston and Logan, 2004). The development time and geological characteristics of these two contrasting types of BIFs strongly demonstrate that the hydrosphere–atmosphere system was rapidly oxidized during 2.33–2.06 Ga.

The carbonate strata have a relatively simple process of origin and are widely developed in the Paleoproterozoic, and can therefore serve as a fingerprint to trace Paleoproterozoic environmental change. As indicated by the REY signature, the Guanmenshan Formation records the environmental change during 2.3–2.06 Ga. The samples of the Guanmenshan Formation differ from the Archean or Phanerozoic chemical sediments by lower positive La anomalies, but are in accordance with those of the 2.10–2.02 Ga South Dakota BIF (Frei et al., 2008; Fig. 9A). The Ce_{SN}/Ce_{SN}^* values of the Guanmenshan Formation dolomicrite range from 0.80 to 1.08, with average of 0.93 ± 0.09, more negative than those of the Archean samples, but the values markedly less than those of Phanerozoic seawater and marine sediments (Figs. 9A, 12; Table 2). The Eu_{SN}/Eu_{SN}^* ratios of the Guanmenshan Formation range 1.34–2.55, corresponding to Eu_{CN}/Eu_{CN}^* = 0.84–1.64, just right around Eu_{SN}/Eu_{SN}^* = 1.53 or Eu_{CN}/Eu_{CN}^* = 1, clearly lower than those of most pre-2.33 Ga chemical sediments (Fig. 15A; Table 2), which suggests that the Guanmenshan Formation developed at the turning point of the Earth's surface environmental evolution.

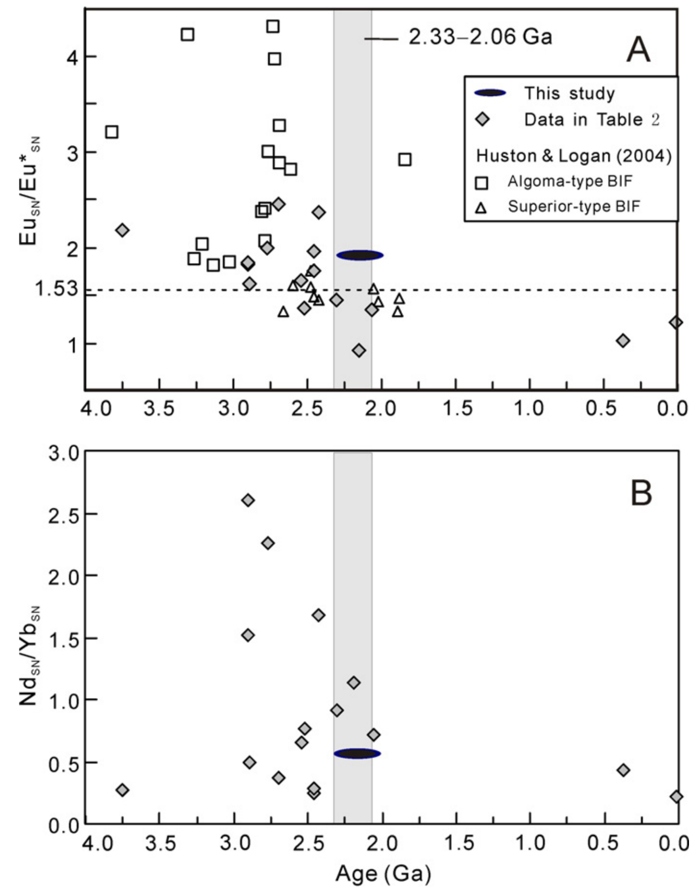

Fig. 15. Chemical sedimentary Eu_{SN}/Eu_{SN}^* and Nd_{SN}/Yb_{SN} and their change with geologic time. Data from Huston and Logan (2004) (n = 158) and Table 2 (n = 205).

To explain the positive-to-negative transition of the sedimentary Eu_{CN}/Eu_{CN}^* anomalies and the decrease of the Nd_{SN}/Yb_{SN} (Fig. 15B) or $(LREE/HREE)_{SN}$, several geochemical models have been proposed (e.g., Taylor and McLennan, 1985; Fryer, 1977; Condie, 1997).

On the basis of the SHAB theory (Dai, 1987), Chen and Zhao (1997) discussed the mechanism of the change in Eu anomalies at around 2.3 Ga. Eu^{2+} and Eu^{3+} are the two natural states of the element Eu. The Eu^{3+}/Eu^{2+} is affected by fO_2; when fO_2 is low, the aqueous anions will prevail as soft bases such as HS^-, S^{2-}, SCN^-, $S_2O_3{}^{2-}$, CO, CH_4; and the value of Eu^{3+}/Eu^{2+} is low; thus Eu is dominated by Eu^{2+}. As a kind of acid, low valence Eu^{2+} is softer than R^{3+} (trivalent REE ions, including Eu^{3+}) which are all typical hard acids. Eu^{2+} is easier than R^{3+} to combine with soft bases into stable complexes and to precipitate from water, whereas R^{3+} prefers to stay in water as ion. Thus sediment deposition in the reducing environment would be characterized by low $\sum$REE and positive Eu-anomaly. On the contrary, when fO_2 is high, Eu is dominated by Eu^{3+} and the anions will be hard bases such as OH^-, $CO_3{}^{2-}$, $SO_4{}^{2-}$ and $NO_3{}^-$. As hard acids, Eu^{3+} and other R^{3+} tend

Please cite this article in press as: Tang, H.-S., et al., REE geochemistry of carbonates from the Guanmenshan Formation, Liaohe Group, NE Sino-Korean Craton: Implications for seawater compositional change during the Great Oxidation Event. Precambrian Res. (2012), doi:10.1016/j.precamres.2012.02.005

to be combined with the hard bases (particularly OH^-) into stable complexes and precipitate, and Eu^{2+} is likely to stay in water. Consequently, the sediments deposited under oxidizing conditions would be characterized by high $\sum$REE and Eu-depletion. Similarly, compared with LR^{3+}, the HR^{3+} are harder acids with smaller ionic radii. The LR^{3+}/HR^{3+} ratios will be high in the reducing environment and low under oxidizing conditions. Therefore, $Eu_{SN}/Eu_{SN}^* > 1.53$ and high Nd_{SN}/Yb_{SN} ratios of the chemical sediments indicate that the depositional environment is reducing whereas those chemical sediments with $Eu_{SN}/Eu_{SN}^* < 1.53$ and low Nd_{SN}/Yb_{SN} ratios are deposited in an oxidizing environment.

In the light of the mechanism discussed above and the REY patterns of the worldwide chemical sediments of different ages, we can confirm that the surficial environment changed from reducing to oxidizing during 2.33–2.06 Ga and a rapid oxidation began at ~2.33 Ga, which is also be supported by the mass development of the evaporite deposits, Superior-type BIF, REE deposits, red beds, carbonates strata, phosphates, stromatolites, graphite deposits and other important changes after 2.3 Ga (Tu et al., 1985; Chen, 1990, 1996; Chen et al., 1991, 1994; Bekker et al., 2003a,b). These inferences are also consistent with about the data from the Lamagundi/Jatulian Event (Schidlowski et al., 1975; Karhu and Holland, 1996; Melezhik et al., 1999).

6. Concluding remarks

(1) The major and trace element geochemical features indicate that the samples examined in this study from the Guanmenshan Formation are typical pure marine chemical sediments. The least altered dolomicrite samples (>600m strata) have $\sum$REE content of 0.739–4.175 ppm (2.414 ± 1.184 ppm, $n = 15$), similar to those of the contemporaneous marine chemical sediments in the world. Their La_{SN}/La_{SN}^*, Gd_{SN}/Gd_{SN}^*, Y/Ho and Nd_{SN}/Yb_{SN} are 0.69–1.90 (1.04 ± 0.27), 1.11–1.60 (1.35 ± 0.16), 34.5–56.6 (44.1 ± 5.7) and 0.24–0.92 (0.56 ± 0.19), respectively, consistent with marine chemical sediments and similar to modern sea water, suggesting that the sea water REY patterns of the Lomagundi period (2.33–2.06 Ga) have been preserved.

(2) The 15 (silicified) dolomicrite samples from the Guanmenshan mining camp and three intensely recrystallized dolomicrite samples with veinlets from the Xiaoxigou mining campus show REY patterns (Eu_{CN}/Eu_{CN}^* ranging 0.83–4.45, and averaging 1.56 ± 0.95; $n = 15$) similar to the high-temperature hydrothermal fluids (>250 °C). They are characterized by flat pattern with striking positive Eu anomalies, suggesting that part of dolostone stratum was metasomatized by high-temperature hydrothermal fluids. These REY patterns record the properties of mineralized fluids.

(3) The Sm_{CN}/Yb_{CN} (>1) of the Guanmenshan Formation are higher than those of the Archean (>2.33 Ga) chemical sediments ($Sm_{CN}/Yb_{CN} < 1$), and suggest that the seafloor hydrothermal fluid had no notable contribution to the REY patterns of the carbonates in the Guanmenshn Formation. The average Eu_{SN}/Eu_{SN}^* of dolomicrite samples is 1.93 ± 0.45 ($n = 15$), or $Eu_{CN}/Eu_{CN}^* \approx 1$ (1.20 ± 0.29), and the average Ce_{SN}/Ce_{SN}^* is 0.93 ± 0.09, indicating that the Guanmenshan Formation was deposited at a critical turning point in the Earth history when the atmosphere–hydrosphere system sharply changed from reducing to oxidizing with a marked increase in the fO_2 of sea water.

Acknowledgments

This study was funded by the National 973-Program (Project nos. 2012CB416602, 2006CB403508), National Natural Science Foundation of China (nos. 40352003, 40425006) and Frontier Field Project of the State Key Laboratory of Ore Deposit Geochemistry, Institute of Geochemistry, Chinese Academy of Sciences, as well as Open Research Foundation of the State Key Laboratory for Mineral Deposits Research, Nanjing University. We wish to sincerely thank Prof. Z.T. Li of the Shenyang Geological Survey, general engineers W. He and Y.F. Qu of the no. 5 geological team of Liaoning Province, and Y.G. Jing, deputy director of the Chemical and Geological Survey, Liaoning Province, for their help in the field investigations. Profs. S.Y. Jiang and Y.P. Lin of the Nanjing University directed the laboratory work. In addition, we wish to thank Dr. Y. H. Lu of the Peking University and Profs. H. Zhang of the Institute of Geochemistry Chinese Academy of Sciences for their valuable discussions. Constructive suggestions, pertinent comments and careful corrections by professors F. Pirajno and two anonymous reviewers greatly improved the quality of the manuscript.

References

Alexander, B.W., Bau, M., Andersson, P., Dulski, P., 2008. Continentally-derived solutes in shallow Archean seawater: rare earth element and Nd isotope evidence in iron formation from the 2.9 Ga Pongola Supergroup, South Africa. Geochim. Cosmochim. Acta 72, 378–394.

Alibo, D.S., Nozaki, Y., 1999. Rare earth elements in seawater: particle association, shale-normalization, and Ce oxidation. Geochim. Cosmochim. Acta 63, 363–372.

Anbar, A.D., Duan, Y., Lyons, T.W., Arnold, G.L., Kendall, B., Creaser, R.A., Kaufman, A.J., Gordon, G.W., Scott, C., Garvin, J., Buick, R., 2007. A whiff of oxygen before the Great Oxidation Event? Science 317, 1903–1906.

Andersson, K., Dahlqvist, R., Turner, D., Stolpe, B., Larsson, T., Ingri, J., Andersson, P., 2006. Colloidal rare earth elements in a boreal river: changing sources and distributions during the spring flood. Geochim. Cosmochim. Acta 70, 3261–3274.

Banner, J.L., Hanson, G.N., 1990. Calculation of simultaneous isotopic and trace element variations during water–rock interaction with applications to carbonate diagenesis. Geochim. Cosmochim. Acta 54, 3123–3137.

Bau, M., Dulski, P., 1996. Distribution of yttrium and rare-earth elements in the Penge and Kuruman iron-formations, Transvaal Supergroup, South Africa. Precambrian Res. 79, 37–55.

Bau, M., Dulski, P., 1999. Comparing yttrium and rare earths in hydrothermal fluids from the Mid-Atlantic Ridge: implications for Y and REE behaviour during near-vent mixing and for the Y/Ho ratio of Proterozoic seawater. Chem. Geol. 155, 77–90.

Bau, M., Möller, P., 1993. Rare earth element systematics of the chemically precipitated component in Early Precambrian iron formations and the evolution of the terrestrial atmosphere–hydrosphere–lithosphere system. Geochim. Cosmochim. Acta 57, 2239–2249.

Bau, M., Koschinsky, A., Dulski, P., Hein, J.R., 1996. Comparison of the partitioning behaviours of yttrium, rare earth elements, and titanium between hydrogenetic marine ferromanganese crusts and seawater. Geochim. Cosmochim. Acta 60, 1709–1725.

Bau, M., Romer, R.L., Lüders, V., Beukes, N.J., 1999. Pb, O, and C isotopes in silicified Mooidraai dolomite (Transvaal Supergroup, South Africa): implications for the composition of Paleoproterozoic seawater and 'dating' the increase of oxygen in the Precambrian atmosphere. Earth Planet. Sci. Lett. 174, 43–57.

Bau, M., Usui, A., Pracejus, B., Mita, N., Kanai, Y., Irber, W., Dulski, P., 1998. Geochemistry of low-temperature water–rock interaction: evidence from natural waters, andesite, and ironoxyhydroxide precipitates at Nishiki-numa iron-spring, Hokkaido, Japan. Chem. Geol. 151, 293–307.

Bau, M., 1991. Rare earth element mobility during hydrothermal and metamorphic fluid–rock interaction and the significance of the oxidation state of europium. Chem. Geol. 93, 219–230.

Bau, M., 1993. Effects of syn- and post-depositional processes on the rare-earth element distribution in Precambrian iron-formations. Eur. J. Mineral. 5, 257–267.

Bau, M., 1996. Controls on fractionation of isovalent trace elements in magmatic and aqueous systems: Evidence from Y/Ho, Zr/Hf, and lanthanide tetrad effect. Contrib. Mineral. Petrol. 123, 323–333.

Bau, M., 1999. Scavenging of dissolved yttrium and rare earths by precipitating iron oxyhydroxide: experimental evidence for Ce oxidation, Y–Ho fractionation, and lanthanide tetrad effect. Geochim. Cosmochim. Acta 63, 67–77.

Bekker, A., Eriksson, K.A., 2003. A Paleoproterozoic drowned carbonate platform on the southeastern margin of the Wyoming Craton: a record of the Kenorland breakup. Precambrian Res. 120, 327–364.

Bekker, A., Karhu, J.A., Eriksson, K.A., Kaufman, A.J., 2003a. Chemostratigraphy of Palaeoproterozoic carbonate successions of the Wyoming Craton: tectonic forcing of biogeochemical change? Precambrian Res. 120, 279–325.

Bekker, A., Karhu, J.A., Kaufman, A.J., 2006. Carbon isotope record for the onset of the Lomagundi carbon isotope excursion in the Great Lakes area, North America. Precambrian Res. 148, 145–180.

Bekker, A., Kaufman, A.J., Karhu, J.A., Beukes, N.J., Swart, Q.D., Coetzee, L.L., Eriksson, K.A., 2001. Chemostratigraphy of the Paleoproterozoic Duitschland Formation, South Africa: implications for coupled climate change and carbon cycling. Am. J. Sci. 301, 261–285.

Bekker, A., Kaufman, A.J., Karhu, J.A., Eriksson, K.A., 2005. Evidence for Paleoproterozoic cap carbonates in North America. Precambrian Res. 137, 167–206.
Bekker, A., Sial, A.N., Karhu, J.A., Ferrerira, V.P., Noce, C.M., Kaufman, A.J., Romano, A.W., Pimentel, M.M., 2003b. Chemostratigraphy of carbonates from the Minas Supergroup, Quadril'atero Ferr'ıfero (Iron Quadrangle), Brazil: a stratigraphic record of early Proterozoic atmospheric, biogeochemical and climatic change. Am. J. Sci. 303, 865–904.
Bhatia, M.R., Crook, K.A.W., 1986. Trace element characteristics of graywackes and tectonic discrimination of sedimentary basins. Contrib. Mineral. Petrol. 92, 181–193.
Bhatia, M.R., 1983. Plate tectonics and geochemical composition of sandstones. J. Geol. 91, 611–627.
Bolhar, R., Kamber, B.S., Moorbath, S., Fedo, C.M., Whitehouse, M.J., 2004. Characterisation of early Archaean chemical sediments by trace element signatures. Earth Planet. Sci. Lett. 222, 43–60.
Bolhar, R., Van Kranendonk, M.J., 2007. A non-marine depositional setting for the northern Fortescue Group, Pilbara Craton, inferred from trace element geochemistry of stromatolitic carbonates. Precambrian Res. 155, 229–250.
Brand, U., Veizer, J., 1980. Chemical diagenesis of a multicomponent carbonate system. 1. Trace elements. J. Sedim. Petrol. 50, 1219–1236.
Buick, I.S., Uken, R., Gibson, R.L., Wallmach, T., 1998. High $\delta^{13}C$ Paleoproterozoic carbonates from the Transvaal Supergroup, South Africa. Geology 26, 875–878.
Byrne, R.H., Lee, J.H., 1993. Comparative yttrium and rare earth element chemistries in seawater. Mar. Chem. 44, 121–130.
Byrne, R.H., Liu, X., Schijf, J., 1996. The influence of phosphate coprecipitation on rare earth element distributions in natural waters. Geochim. Cosmochim. Acta 60, 3341–3346.
Chen, C.X., Cai, K.Q., 2000. Minerogenic system of magnesian nonmetalliic deposits in early Proterozoic Mg-rich carbonate formations in eastern Liaoning Province. Acta Geol. Sin. 74, 623–631.
Chen, Y.J., Fu, S.G., Hu, S.X., Zhang, Y.Y., 1992. The REE geochemical evolution and its significance of the Wuyang early Precambrian metamorphic terrain. Chin. J. Geochem. 11, 133–139.
Chen, Y.J. (Ed.), 1996. Current progresses in indications of crustal composition and sedimentary environment and their evolutions with sedimentary trace elements. Geol. Geochem. 3, 1–125 (in Chinese).
Chen, Y.J., 1988. Catastrophe of the geologic environment at 2300 Ma. In: Abstracts of International Symposium on Geochemistry and Mineralization of Proterozoic Mobile Belts, Tianjin, September 6–10, p. p11.
Chen, Y.J., 1990. Evidences for the catastrophe in geologic environment at about 2300 Ma and the discussions on several problems. J. Stratigr. 14, 178–186 (in Chinese with English abstract).
Chen, Y.J., Fu, S.G., 1991. Variation of REE patterns in early Precambrian sediments: theoretical study and evidence from the southern margin of the northern China Craton. Chin. Sci. Bull. 36, 1100–1104.
Chen, Y.J., Fu, S.G., 1992. Gold Mineralization in West Henan. Chinese Seismological Press, Beijing, 234 p. (in Chinese with English abstract).
Chen, Y.J., Hu, S.X., Lu, B., 1998. Contrasting REE geochemical features between Archean and Proterozoic khondalite series in North China Craton. Mineral. Mag. 62A (1), 318–319.
Chen, Y.J., Ji, H.Z., Zhou, X.P., Fu, S.G., 1991. The challenge to the traditional geological theories from revelation of the catastrophe at 2300 Ma: new knowledge on several important geological subjects. Adv. Earth Sci. 6 (2), 63–68 (in Chinese with English abstract).
Chen, Y.J., Liu, C.Q., Chen, H.Y., Zhang, Z.J., Li, C., 2000. Carbon isotope geochemistry of graphite deposits and ore-bearing khondalite series in North China: implications for several geoscientific problems. Acta Petrol. Sin. 16, 233–244 (in Chinese with English abstract).
Chen, Y.J., Ouyang, Z.Y., Yang, Q.J., Deng, J., 1994. A new understanding of the Archean–Proterozoic boundary. Geol. Rev. 40, 483–488 (in Chinese with English abstract).
Chen, Y.J., Su, S.G., 1998. Catastrophe in geological environment at 2300 Ma. Mineral. Mag. 62A (1), 320–321.
Chen, Y.J., Yang, J.Q., Deng, J., Ji, H.Z., Fu, S.G., Zhou, X.P., Lin, Q., 1996. An important change in Earth's evolution: an environmental catastrophe at 2300 Ma and its implications. Geol. Geochem. 3, 106–128 (in Chinese).
Chen, Y.J., Zhao, Y.C., 1997. Geochemical characteristics and evolution of REE in the Early Precambrian sediments: evidences from the southern margin of the North China Craton. Episodes 20, 109–116.
Condie, K.C., 1997. Plate Tectonics and Crustal Evolution. Butterworth-Heinemann, Oxford, 282 p.
Dai, A.B., 1987. Coordination Chemistry. Science Press, Beijing, 870 p. (in Chinese).
De Baar, H.J.W., Bacon, M.P., Brewer, P.G., 1985. Rare earth elements in the Pacific and Atlantic Oceans. Geochim. Cosmochim. Acta 49, 1943–1959.
Derry, L.A., Jacobsen, S.B., 1990. The chemical evolution of Precambrian seawater: evidence from rare earth elements in banded iron formations. Geochim. Cosmochim. Acta 54, 2965–2977.
Elderfield, H., Upstill-Goddard, R., Sholkovitz, E.R., 1990. The rare earth elements in rivers, estuaries, and coastal seas and their significance to the composition of ocean waters. Geochim. Cosmochim. Acta 54, 971–991.
Erel, Y., Stolper, E.M., 1993. Modeling of rare-earth element partitioning between particles and solution in aquatic environments. Geochim. Cosmochim. Acta 57, 513–518.
Frei, R., Dahl, P.S., Duke, E.F., Frei, K.M., Hansen, T.R., Frandsson, M.M., Jensen, L.A., 2008. Trace element and isotopic characterization of Neoarchean and Paleoproterozoic iron formations in the Black Hills (South Dakota, USA): assessment of chemical change during 2.9–1.9 Ga deposition bracketing the 2.4–2.2 Ga first rise of atmospheric oxygen. Precambrian Res. 162, 441–474.
Fryer, B., 1977. Rare-earth evidence in iron-formations for changing Precambrian oxidation states. Geochim. Cosmochim. Acta 41, 361–367.
Girty, G.H., Harnson, A.D., Knaack, C., Johnson, D., 1994. Provenance determined by REE, Th, and Sc analyses of metasedimentary rocks, Boyden Cave Pendant, central Siena Nevada, California. J. Sedim. Res. B64 (1), 68–73.
Goldstein, S.J., Jacobsen, S.B., 1988. Rare earth elements in river waters. Earth Planet. Sci. Lett. 89, 35–47.
Gross, G.A., 1983. Tectonic systems and the deposition of iron formation. Precambrian Res. 20, 171–187.
Guo, J.H., O'Brien, P.J., Zhai, M.G., 2002. High-pressure granulites in the Sanggan area, North China Craton: metamorphic evolution, P–T paths and geotectonic significance. J. Metamorph. Geol. 20, 741–756.
Guo, J.H., Sun, M., Zhai, M.G., 2005. Sm–Nd and SHRIMP U–Pb zircon geochronology of high-pressure granulites in the Sanggan area, North China Craton: timing of Paleoproterozoic continental collision. J. Asian Earth Sci. 24, 629–642.
Hannigan, R.E., Sholkovitz, E.R., 2001. The development of middle rare earth element enrichments in freshwaters: weathering of phosphate minerals. Chem. Geol. 175, 495–508.
Huston, D.L., Logan, G.A., 2004. Barite, BIFs and bugs: evidence for the evolution of the Earth's early atmosphere. Earth Planet. Sci. Lett. 220, 41–55.
Jacobsen, S.B., Kaufman, A.J., 1999. The Sr, C and O isotopic evolution of Neoproterozoic seawater. Chem. Geol. 161, 37–57.
Jiang, C.C., 1984. A rewiew of the Precambrian stratigraphic division and correlation of eastern parts of Liaoning and Jilin. Acta Geosci. Sin. 9, 157–167 (in Chinese with English abstract).
Jiang, S.Y., Chen, C.X., Chen, Y.Q., Jiang, Y.H., Dai, B.Z., Ni, P., 2004. Geochemistry and genetic model for the giant magnesite deposits in the eastern Liaoning province, China. Acta Petrol. Sin. 20, 765–772 (in English with Chinese abstract).
Jiang, S.Y., Palmer, M.R., Peng, Q.M., Yang, J.H., 1997. Chemical and stable isotope (B, Si, and O) compositions of Proterozoic metamorphosed evaporite and associated tourmalines from the Houxianyu borate deposit, eastern Liaoning, China. Chem. Geol. 135, 189–211.
Kamber, B.S., Webb, G.E., 2001. The geochemistry of late Archaean microbial carbonate: implications for ocean chemistry and continental erosion history. Geochim. Cosmochim. Acta 65, 2509–2525.
Karhu, J.A., Holland, H.D., 1996. Carbon isotopes and the rise of atmospheric oxygen. Geology 24, 867–870.
Konhauser, K.O., Pecoits, E., Lalonde, S.V., Papineau, D., Nisbet, E.G., Barley, M.E., Arndt, N.T., Zahnle, K., Kamber, B.S., 2009. Oceanic nickel depletion and a methanogen famine before the Great Oxidation Event. Nature 458, 750–753.
Kröner, A., Wilde, S.A., Li, J.H., Wang, K.Y., 2005. Age and evolution of a late Archean to Early Palaeozoic upper to lower crustal section in the Wutaishan/Hengshan/Fuping terrain of northern China. J. Asian Earth Sci. 24, 577–595.
Kröner, A., Wilde, S.A., Zhao, G.C., O'Brien, P.J., Sun, M., Liu, D.Y., Wan, Y.S., Liu, S.W., Guo, J.H., 2006. Zircon geochronology of mafic dykes in the Hengshan Complex of northern China: evidence for Late Paleoproterozoic rifting and subsequent high-pressure event in the North China Craton. Precambrian Res. 146, 45–67.
Kusky, T.M., 2011. Geophysical and geological tests of tectonic models of the North China Craton. Gondwana Res. 20, 26–35.
Lee, J.H., Byrne, R.H., 1992. Complexation of trivalent rare earth elements (Ce, Eu, Gd, Tb, Yb) by carbonate ions. Geochim. Cosmochim. Acta 57, 295–302.
Li, S.Z., Zhao, G.C., 2007. SHRIMP U–Pb zircon geochronology of the Liaoji granitoids: constraints on the evolution of the Paleoproterozoic Jiao-Liao-Ji belt in the Eastern Block of the North China Craton. Precambrian Res. 158, 1–16.
Li, S.Z., Zhao, G.C., Sun, M., Wu, F.Y., Liu, J.Z., Hao, D.F., Han, Z.Z., Luo, Y., 2004. Mesozoic, not Paleoproterozoic SHRIMP U–Pb zircon ages of two Liaoji granites, Eastern Block, North China Craton. Int. Geol. Rev. 46, 162–176.
Li, S.Z., Zhao, G.C., Sun, M., Han, Z.Z., Luo, Y., Hao, D.F., Xia, X.P., 2005. Deformation history of the Paleoproterozoic Liaohe assemblage in the eastern block of the North China Craton. J. Asian Earth Sci. 24, 659–674.
Li, S.Z., Zhao, G.C., Sun, M., Han, Z.Z., Zhao, G.T., Hao, D.F., 2006. Are the South and North Liaohe Groups of the North China Craton different exotic terranes? Nd isotope constraints. Gondwana Res. 9, 198–208.
Liaoning Bureau of Geology and Mineral Resources, 1989. The Regional Geology of Liaoning Province. Geological Publishing House, Beijing, 856 p. (in Chinese with English abstract).
Liu, S.W., Zhao, G.C., Wilde, S.A., Shu, G.M., Sun, M., Li, Q.G., Tian, W., Zhang, J., 2006. Th–U–Pb monazite geochronology of the Lüliang and Wutai Complexes: constraints on the tectonothermal evolution of the Trans-North China Orogen. Precambrian Res. 148, 205–224.
Liu, Y., Liu, H.C., Li, X.H., 1996. Simultaneous and precise determination of 40 trace elements in rock samples using ICP-MS. Geochimica 25, 552–558 (in Chinese with English abstract).
Liu, C., Zhao, G.C., Sun, M., Zhang, J., He, Y., Yin, C., Wu, F., Yang, J., 2011. U–Pb and Hf isotopic study of detrital zircons from the Hutuo group in the Trans-North China Orogen and tectonic implications. Gondwana Res. 20, 106–121.
McLennan, S.M., 1989. Rare earth elements in sedimentary rocks: influence of provenance and sedimentary processes. In: Lipin, B.R., McKay, G.A. (Eds.), Geochemistry and Mineralogy of Rare Earth Elements, vol. 21. Rev. Mineral., Mineral. Soc. Am., pp. 169–200.
Melezhik, V.A., Bingen, B., Fallick, A.E., Gorokhov, I.M., Kuznetsov, A.B., Sandstad, J.S., Solli, A., Bjerkgård, T., Henderson, I., Boyda, R., Jamal, D., Monize, A., 2008.

Isotope chemostratigraphy of marbles in northeastern Mozambique: apparent depositional ages and tectonostratigraphic implications. Precambrian Res. 162, 540–558.
Melezhik, V.A., Fallick, A.E., 1996. A widespread positive $\delta^{13}C_{carb}$ anomaly at 2.33–2.06 Ga on the Fennoscandian Shield: a paradox? Terra Nova 8, 141–157.
Melezhik, V.A., Fallick, A.E., Clark, A., 1997. Two billion year old isotopically heavy carbon: evidence from the Labrador Trough, Canada. Can. J. Earth Sci. 34, 271–285.
Melezhik, V.A., Fallick, A.E., Medvedev, P.V., Makarikhin, V.V., 1999. Extreme $^{13}C_{carb}$ enrichment in ca.2.0 Ga magnesite–stromatolite–dolomite-'red beds' association in a global context: a case for the worldwide signal enhanced by a local environment. Earth Sci. Rev. 48, 71–120.
Melezhik, V.A., Gorokhov, I.M., Fallick, A.E., Gjelle, S., 2001a. Strontium and carbon isotope geochemistry applied to dating of carbonate sedimentation: an example from high-grade rocks of the Norwegian Caledonides. Precambrian Res. 108, 267–292.
Melezhik, V.A., Gorokhov, I.M., Kuznetsov, A.B., Fallick, A.E., 2001b. Review article: chemostratigraphy of Neoproterozoic carbonates: implications for 'blind dating'. Terra Nova 13, 1–11.
Melezhik, V.A., Kuznetsov, A.B., Fallick, A.F., Smith, R.A., Gorokhov, I.M., Jamal, D., Catuane, F., 2006. Depositional environments and an apparent age for the Geci meta-limestones: constraints on the geological history of northern Mozambique. Precambrian Res. 148, 19–31.
Melezhik, V.A., Roberts, D., Fallick, A.E., Gorokhov, I.M., Kuznetsov, A.B., 2005. Geochemical preservation potential of high-grade calcite marble versus dolomite marble: implication for isotope chemostratigraphy. Chem. Geol. 216, 203–224.
Möller, P., Bau, M., 1993. Rare-earth patterns with positive cerium anomaly in alkaline waters from Lake Van, Turkey. Earth Planet. Sci. Lett. 117, 671–676.
Nesbitt, H.W., MacRae, N.D., Kronberg, B.I., 1990. Amazon deep-sea fan muds: light REE enriched products of exteme chemical weathering. Earth Planet. Sci. Lett. 100, 118–123.
Nothdurft, L.D., Webb, G.E., Kamber, B.S., 2004. Rare earth element geochemistry of Late Devonian reefal carbonates, Canning Basin, Western Australia: confirmation of a seawater REE proxy in ancient limestones. Geochim. Cosmochim. Acta 68, 263–283.
Nozaki, Y., Zhang, Y.S., Amakawa, H., 1997. The fractionation between Y and Ho in the marine environment. Earth Planet. Sci. Lett. 148, 329–340.
Pichler, T., Veizer, J., Hall, G.E.M., 1999. The chemical composition of shallow-water hydrothermal fluids in Tutum Bay, Ambitle Island, Papua New Guinea and their effect on ambient seawater. Mar. Chem. 64, 229–252.
Rui, Z.Y., Li, N., Wang, L.S., 1991. Lead and Zinc Deposits of Guanmenshan. Geological Publishing House, Beijing, 208 p. (in Chinese with English abstract).
Santosh, M., Sajeev, K., Li, J.H., 2006. Extreme crustal metamorphism during Columbia supercontinent assembly: evidence from North China Craton. Gondwana Res. 10, 256–266.
Santosh, M., Tsunogae, T., Li, J.H., 2007a. Discovery of sapphirine-bearing Mg–Al granulites in the North China Craton: implications for Paleoproterozoic ultrahigh temperature metamorphism. Gondwana Res. 11, 263–285.
Santosh, M., Wilde, S.A., Li, J.H., 2007b. Timing of Paleoproterozoic ultrahigh-temperature metamorphism in the North China Craton: evidence from SHRIMP U–Pb zircon geochronology. Precambrian Res. 159, 178–196.
Santosh, M., Tsunogae, T., Ohyama, H., Sato, K., Li, J.H., Liu Liu, S.J., 2008. Carbonic metamorphism at ultrahigh-temperatures: evidence from North China Craton. Earth Planet. Sci. Lett. 266, 149–165.
Santosh, M., Sajeev, K., Li, J.H., Liu, S.J., Itaya, T., 2009. Counterclockwise exhumation of a hot orogen: the Paleoproterozoic ultrahigh-temperature granulites in the North China Craton. Lithos 110, 140–152.
Santosh, M., 2010. Assembling North China Craton within the Columbia supercontinent: the role of double-sided subduction. Precambrian Res. 178, 149–167.
Santosh, M., Liu, S.J., Tsunogae, T., Li, J.H., 2011. Paleoproterozoic ultrahigh-temperature granulites in the North China Craton: implications for tectonic models on extreme crustal metamorphism. Precambrian Res., doi:10.1016/j.precamres.2011.05.003.
Schidlowski, M., 1988. A 3800-million-year isotopic record of life from carbon in sedimentary rocks. Nature 333, 313–318.
Schidlowski, M., Eichmann, R., Junge, C.E., 1975. Precambrian sedimentary carbonates: carbon and oxygen isotope geochemistry and implications for the terrestrial oxygen budget. Precambrian Res. 2, 1–69.
Schidlowski, M., Eichmann, R., Junge, C.E., 1976. Carbon isotope geochemistry of the Precambrian Lomagundi carbonate province Rhodesia. Geochim. Cosmochim. Acta 40, 449–455.
Shields, G., Stille, P., 2001. Diagenetic constraints on the use of cerium anomalies as palaeoseawater redox proxies: an isotopic and REE study of Cambrian phosphorites. Chem. Geol. 175, 29–48.
Shields, G.A., Webb, G.E., 2004. Has the REE composition of seawater changed over geological time? Chem. Geol. 204, 103–107.
Sholkovitz, E., Szymczak, R., 2000. The estuarine chemistry of rare earth elements: comparison of the Amazon, Fly, Sepik and the Gulf of Papua systems. Earth Planet. Sci. Lett. 179, 299–309.
Sholkovitz, E.R., Landing, W.M., Lewis, B.L., 1994. Ocean particle chemistry: the fractionation of rare earth elements between suspended particles and seawater. Geochim. Cosmochim. Acta 58, 1567–1579.
Song, B., Qiao, X.F., 2008. Ages of the zircons from basalt of the Erdaogou Formation and diabase dyke warms in Northern Liaoning, and their significances. Earth Sci. Front. 15, 250–262.
Sun, M., Armstrong, R.L., Lambert, R.S., Jiang, C.C., Wu, J.H., 1993. Petrochemistry and Sr, Pb and Nd isotopic geochemistry of Paleoproterozoic Kuandian Complex, the eastern Liaoning Province, China. Precambrian Res. 62, 171–190.
Sun, M., Zhang, L.F., Wu, J.H., 1996. The origin of the early proterozoic Kuandian Complex: evidence from geochemistry. Acta Geol. Sin. 70, 207–222 (in Chinese with English abstract).
Tam, P.Y., Zhao, G.C., Liu, F., Zhou, X., Sun, M., Li, S.Z., 2011. Timing of etamorphismin the Paleoproterozoic Jiao-Liao-Ji Belt: new SHRIMP U–Pb zircon dating of granulites, gneisses and marbles of the Jiaobei massif in the North China Craton. Gondwana Res. 19, 150–162.
Tang, G.J., Chen, Y.J., Huang, B.L., Chen, C.X., 2004. Paleoprotoerozoic $\delta^{13}C_{carb}$ positive excursion event: research progress on 2.3 Ga catastrophe. J. Mineral. Petrol. 24 (3), 103–109 (in Chinese with English abstract).
Tang, H.S., Chen, Y.J., Wu, G., Lai, Y., 2011. Paleoproterozoic positive $\delta^{13}C_{carb}$ excursion in northeastern Sino-Korean Craton: evidence of the Lomagundi Event. Gondwana Res. 19, 471–481.
Tang, H.S., Wu, G., Lai, Y., 2009. The C–O isotope geochemistry and genesis of the Dashiqiao magnesite deposit, Liaoning province, NE China. Acta Petrol. Sin. 25, 455–467 (in Chinese with English abstract).
Taylor, S.R., McLennan, S.M., 1985. The Continental Crust: Its Composition and Evolution. Blackwell, Oxford, 312 p.
Tsunogae, T., Liu, S.J., Santosh, M., Shimuzu, H., Li, J.H., 2011. Ultrahigh-temperature metamorphism in Daqingshan, Inner Mongolia Suture Zone North China Craton. Gondwana Res. 20, 36–47.
Tu, G.C., Zhao, Z.H., Qiu, Y.Z., 1985. Evolution of Precambrian REE mineralization. Precambrian Res. 27, 131–151.
Van Kranendonk, M.J., Webb, G.E., Kamber, B.S., 2003. New geological and trace element evidence from 3.45 Ga stromatolitic carbonates in the Pilbara Craton: support of a marine, biogenic origin and for a reducing Archaean ocean. Geobiology 1, 91–108.
Veizer, J., Ala, D., Azmy, K., Bruckschen, P., Buhl, D., Bruhn, F., Carden, G.A.F., Diener, A., Ebneth, S., Godderis, Y., Jasper, T., Korte, C., Pawallek, F., Podlaha, O.G., Strauss, H., 1999. $^{87}Sr/^{86}Sr$, $\delta^{13}C$ and $\delta^{18}O$ evolution of Phanerozoic seawater. Chem. Geol. 161, 59–88.
Veizer, J., Clayton, R.N., Hinton, R.W., 1992. Geochemistry of Precambrian carbonates: IV. Early Paleoproterozoic (2.25 ± 0.25 Ga) seawater. Geochim. Cosmochim. Acta 56, 875–885.
Veizer, J., 1983. Chemical diagenesis of carbonates: theory and application of trace element technique. In: Arthur, M.A., Anderson, T.F., Kaplan, I.R., Veizer, J., Land, L.S. (Eds.), Stable Isotopes in Sedimentary Geology, vol.10. Society of Economic Paleontologists and Mineralogists, pp. pp3.1–3.100 (Short Course 10).
Wan, Y.S., Song, B., Liu, D.Y., Wilde, S.A., Wu, J.S., Shi, Y.R., Yin, X.Y., Zhou, H.Y., 2006. SHRIMP U–Pb zircon geochronology of Palaeoproterozoic metasedimentary rocks in the North China Craton: evidence for a major Late Palaeoproterozoic tectonothermal event. Precambrian Res. 149, 249–271.
Wan, Y.S., Liu, D.Y., Wang, W., Song, T., Kröner, A., Dong, C., Zhou, H., Yin, X.Y., 2011. Provenance of Meso- to Neoproterozoic cover sediments at the Ming Tombs, Beijing, North China Craton: An integrated study of U–Pb dating and Hf isotopic measurement of detrital zircons and whole-rock geochemistry. Gondwana Res. 20, 219–242.
Wang, C.Q., Fan, Y.B., Luo, J.M., 1989. The geological characteristics of Proterozoic marine volcanic rocks—spilite in the Xunhe area, Northern Liaoning. Regional Geol. China 30 (3), 237–242.
Webb, G.E., Kamber, B.S., 2000. Rare earth elements in Holocene reefal microbialites: a new shallow seawater proxy. Geochim. Cosmochim. Acta 64, 1557–1565.
Wheat, C.G., Mottl, M.J., Rudnicki, M., 2002. Trace element and REE composition of a low-temperature ridge-flank hydrothermal spring. Geochim. Cosmochim. Acta 66, 3693–3705.
Xia, X.P., Sun, M., Zhao, G.C., Luo, Y., 2006a. LA-ICP-MS U–Pb geochronology of detrital zircons from the Jining Complex, North China Craton and its tectonic significance. Precambrian Res. 144, 199–212.
Xia, X.P., Sun, M., Zhao, G.C., Wu, F.Y., Xu, P., Zhang, J.H., Luo, Y., 2006b. U–Pb and Hf isotopic study of detrital zircons from the Wulashan khondalites: constraints on the evolution of the Ordos Terrane, Western Block of the North China Craton. Earth Planet. Sci. Lett. 241, 581–593.
Yin, C.Q., Zhao, G.C., Sun, M., Xia, X.P., Wei, C.J., Leung, W.H., 2009. LA-ICP-MS U–Pb zircon ages of the Qianlishan Complex: constrains on the evolution of the Khondalite Belt in the Western Block of the North China Craton. Precambrian Res. 174, 78–94.
Zhai, M.G., Santosh, M., 2011. The Early Precambrian odyssey of the North China Craton: a synoptic overview. Gondwana Res. 20, 6–25.
Zhang, J., Zhao, G.C., Sun, M., Wilde, S.A., Li, S.Z., Liu, S.W., 2006. High-pressure mafic granulites in the Trans-North China Orogen: tectonic significance and age. Gondwana Res. 9, 349–362.
Zhang, J., Zhao, G.C., Li, S.Z., Sun, M., Liu, S.W., Wilde, S.A., Kroner, A., Yin, C.Q., 2007. Deformation history of the Hengshan Complex: implications for the tectonic evolution of the Trans-North China Orogen. J. Struct. Geol. 29, 933–949.
Zhang, J., Zhao, G.C., Li, S.Z., Sun, M., Liu, S.W., Yin, C.Q., 2009. Deformational history of the Fuping Complex and new U–Th–Pb geochronological constraints: implications for the tectonic evolution of the Trans-North China Orogen. J. Struct. Geol. 31, 177–193.
Zhao, G.C., Sun, M., Wilde, S.A., Li, S.H., 2004. A Paleo-Mesoproterozoic supercontinent: assembly, growth and breakup. Earth Sci. Rev. 67, 91–123.
Zhao, G.C., Sun, M., Wilde, S.A., Li, S.Z., 2005. Late Archean to Paleoproterozoic evolution of the North China Craton: key issues revisited. Precambrian Res. 136, 177–202.

Zhao, G.C., Sun, M., Wilde, Li, S.Z., Liu, S.W., Zhang, J., 2006. Composite nature of the North China Granulite-Facies Belt: tectonothermal and geochronological constraints. Gondwana Res. 9, 337–348.

Zhang, Q.S., Yang, Z.S., Wang, Y.J., 1988. Early Crust and Mineral Deposits of Liaodong Peninsula. Geological Publishing House, Beijing, 574 p. (in Chinese).

Zhang, X.J., Zhang, L.C., Xiang, P., Wan, B., Prajno, F., 2011. Zircon U–Pb age, Hf isotopes and geochemistry of Shuichang Algoma-type banded iron-formation, North China Craton: Constraints on the ore-forming age and tectonic setting. Gondwana Res. 20, 137–148.

Zhao, Z.H., 2010. Banded iron formation and Great Oxidation Event. Earth Sci. Front. 17, 1–12 (in Chinese with English abstract).